The Hydrogen Bonding and Hydration of 2′-OH in Adenosine and Adenosine 3′-Ethyl Phosphate

Parag Acharya and Jyoti Chattopadhyaya*

Department of Bioorganic Chemistry, Box 581, Biomedical Centre, University of Uppsala, S-751 23 Uppsala, Sweden

jyoti.chattopadhyaya@bioorgchem.uu.se

Received October 1, 2001

The 2′-OH group has major structural implications in the recognition, processing, and catalytic properties of RNA. We report here intra- and intermolecular H-bonding of 2′-OH in adenosine 3′-ethyl phosphate (**1**), 3′-deoxyadenosine (**2**), and adenosine (**3**) by both temperature- and concentration-dependent NMR studies, as well as by detailed endo ($^3J_{H,H}$) and exocyclic ($^3J_{H,OH}$) coupling constant analyses. We have also examined the nature of hydration and exchange processes of 2′-OH with water by a combination of NOESY and ROESY experiments in DMSO-d_6 containing 2 mol % HOD. The NMR-constrained molecular modeling (by molecular mechanics as well as by ab initio methods both in the gas and solution phase) has been used to characterize the energy minima among the four alternative dihedrals possible from the solution of the Karplus equation for $^3J_{H2',OH}$ and $^3J_{H3',OH}$ to delineate the preferred orientation of 2′-O-H proton in **1** and **2** as well as for 2′/3′-O-H protons in **3**. The NMR line shape analysis of 2′-OH gave the ΔG^{H-bond}_{298K} of 7.5 kJ mol^{-1} for **1** and 8.4 kJ mol^{-1} for **3**; similar analyses of the methylene protons of 3′-ethyl phosphate moiety in **1** also gave comparable ΔG^{H-bond}_{298K} of 7.3 kJ mol^{-1}. The donor nature of the 2′-OH in the intramolecular H-bonding in **3** is evident from its relatively reduced flexibility [$-T\Delta S^{\ddagger}]_{2'-OH} = -17.9$ ($\pm$0.5) kJ mol^{-1}] because of the loss of conformational freedom owing to the intramolecular 2′O-H···O3′ H-bonding, compared to the acceptor 3′-OH in **3** [$-T\Delta S^{\ddagger}]_{3'-OH} = -19.8$ ($\pm$ 0.6) kJ mol^{-1}] at 298 K. The presence of intramolecular 2′-OH···O3′ H-bonding in **3** is also corroborated by the existence of weak long-range $^4J_{H2',OH3'}$ in **3** (i.e., W conformation of H2′−C2′−C3′−O3′−H) as well as by $^3J_{H,OH}$ dependent orientation of the 2′- and 3′-OH groups. The ROESY spectra for **1** and **3** at 308 K, in DMSO-d_6, show a clear positive ROE contact of both 2′- and 3′-OH with water. The presence of a hydrophilic 3′-phosphate group in **1** causes a much higher water activity in the vicinity of its 2′-OH, which in turn causes the 2′-OH to exchange faster, culminating in a shorter exchange lifetime (τ) for 2′-OH proton with HOD in **1** ($\tau_{2'-OH}$: 489 ms) compared to that in **3** ($\tau_{2'-OH}$: 6897 ms). The activation energy (E_a) of the exchange with the bound-water for 2′- and 3′-OH in **3** (48.3 and 45.0 kJ mol^{-1}, respectively) is higher compared to that of 2′-OH in **1** (31.9 kJ mol^{-1}), thereby showing that the kinetic availability of hydrated 2′-OH in **1** for any inter- and intramolecular interactions, in general, is owing to the vicinal 3′-phosphate residue. It also suggests that 2′-OH in native RNA can mediate other inter- or intramolecular interactions only in competition with the bound-water, depending upon the specific chemical nature and spatial orientation of other functions with potential for hydrogen bonding in the neighborhood. This availability of the bound water around 2′-OH in RNA would, however, be dictated by whether the vicinal phosphate is exposed to the bulk water or not. This implies that relatively poor hydration around a specific 2′-OH across a polyribonucleotide chain, owing to some hydrophobic microenvironmental pocket around that hydroxyl, may make it more accessible to interact with other donor or acceptor functions for H-bonding interactions, which might then cause the RNA to fold in a specific manner generating a new motif leading to specific recognition and function. Alternatively, a differential hydration of a specific 2′-OH may modulate its nucleophilicity to undergo stereospecific transesterification reaction as encountered in ubiquitous splicing of pre-mRNA to processed RNA or RNA catalysis, in general.

Introduction

The role of RNA is ubiquitous in our cellular information transmission pathway in that it plays distinctive roles in every step from transcription of genes to translation to functional proteins.[1b−d] It has been recently implicated even in the peptide bond formation in the ribosome[1e,f] that RNAs can adopt complex three-dimensional folds, just as protein, to stereochemically and spatially orient its chemical functions in various structural scaffolds to act specifically in various transesterification reactions such as biological catalysis[1j,g] and splicing[1h] or in the translation process.[1b,d] To understand how RNA folds[1i] in various motifs and scaffolds and how these folds generate various cellular functions, we should try to understand the unique role of its 2′-OH group. The 2′-OH group, which distinguishes RNA from DNA, is a

* To whom correspondence should be addressed. Tel: +46 18-471 4577. Fax: +46 18-554-495.

(1) (a) Jeffrey, G. A.; Saenger, W. *Hydrogen Bonding in Biological Systems*; Springer-Verlag: Berlin, 1991. (b) Cech, T. R. *Annu. Rev. Biochem*. **1990**, *59*, 543. (c) Symons, R. H. *Annu. Rev. Biochem*. **1992**, *61*, 641. (d) Brown, R. S.; Hingerty, B. E.; Dewan, J. C.; Klug, A. *Nature* **1983**, *303*, 543. (e) Nissen, P.; Hansen J.; Nenad, B.; Moore, P. B.; Steitz, T. A. *Science* **2000**, *289*, 920. (f) Carter, A. P.; Clemons W. M.; Brodersen, D. E.; Morgan-Warren, R. J.; Wimberly, B. T.; Ramakrishnan V. *Nature* **2000**, *407*, 340. (g) Cate, J. H.; Gooding A. R.; Podell, E.; Zhou, K.; Golden, B.; Doudna J. A. *Science* **1996**, *273*, 1678. (h) Abramovitz, D. L.; Friedman, R. A.; Pyle, A. M. *Science* **1996**, *271*, 1410. (i) Ferré-D'Amaré, A. R.; Doudna J. A. *Annu. Rev. Biophys. Biomol. Struct.* **1999**, *28*, 57. (j) Pyle, A. M.; Cech, T. R., *Nature* **1991**, *350*, 628. (k) Hermann, T.; Patel, D. J. *J. Mol. Biol.* **1999**, *294*, 829. (m) Auffinger, P.; Westhof, E. *J. Mol. Biol.* **1997**, *274*, 54. (n) Schneider, C.; Sühnel, J. *Biopolymer* **1999**, *50*, 287. (p) Egli, M.; Portmann, S.; Usman, N. *Biochemistry* **1996**, *35*, 8489.

10.1021/jo010960j CCC: $22.00
Published on Web 02/16/2002

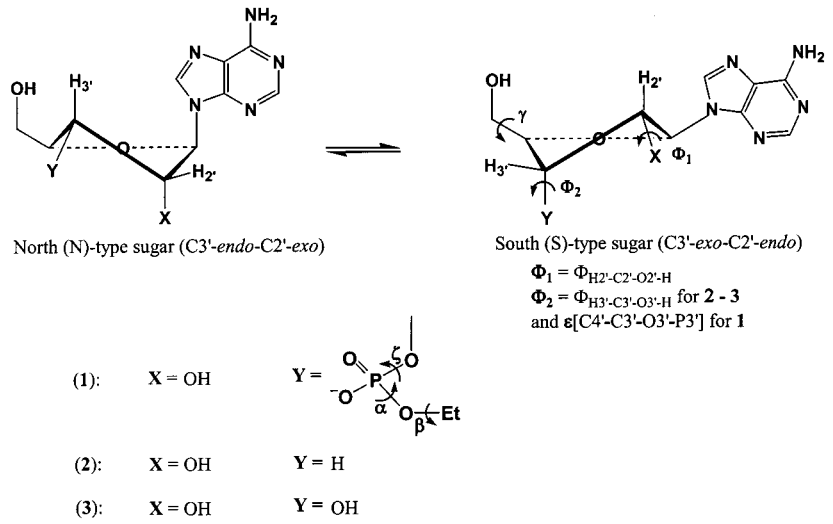

Figure 1. Schematic representation of the bias of the dynamic two-state pseudorotational equilibrium between the north-type (N, C2′-*exo*−C3′-*endo*) and the south-type (S, C3′-*exo*−C2′-*endo*)[5e,f,6a−d,7] pseudorotamers of the sugar moieties of adenosine 3′-ethyl phosphate (**1**), 3′-deoxyadenosine (**2**), and adenosine (**3**). The hydroxyl torsion (Φ) is around the C2′/3′−O bond with $\Phi_1 = \Phi_{H2'-C2'-O2'-H}$ and $\Phi_2 = \Phi_{H3'-C3'-O3'-H}$, except in **1** where the torsion across C3′−O3′ bond is ε^- [C4′−C3′−O3′−P3′]. The major pseudorotamers in **1**−**3** are as follows: S-type in **1**, N-type in **2**, and S-type in **3** (see the PSEUROT[6,7] analyses in the Experimental Section for details).

powerful handle to drive the sugar−phosphate backbone conformation both stereoelectronically[2a] and by direct interaction with the neighboring function, namely intra- as well as intermolecular hydrogen bonding.[1a] It is likely that the reactivity of the 2′-OH group can potentially be influenced by its preferred orientation,[1m] dynamics,[1n] and the pK_a,[2b] which are known to be dictated by various factors such as the nature and orientation of the aglycon,[2b] the sugar conformation,[2b] and the nature of the vicinal substituent.[2b]

To the best of our knowledge, no direct NMR studies have been performed to understand the nature of 2′-OH-mediated intramolecular hydrogen bonding in nucleosides and nucleotides. This is mainly because direct observation of the 2′-OH group under an NMR condition in the aqueous media is impossible because of its free exchange with the solvent. Attempted NMR studies of peptides[2c−f] and monosaccharides[4] also posed similar problems, but they were circumvented by studying the hydrogen-bonding process either in DMSO-d_6 or in $CDCl_3$. Although NMR studies of monosaccharides have been performed previously in DMSO-d_6, this information cannot be however extrapolated to the furanose system because it is comparatively much more flexible due to the lower activation energy barrier[8] for ring inversion [e.g., 20 ± 2 kJ mol^{-1} between north-type (N, C2′-*exo*-C3′-*endo*) and south-type (S, C3′-*exo*-C2′-*endo*) pseudorotamers[5,6a,b,7] (N ⇆ S, Figure 1) in purine nucleosides[8b]] compared to the pyranosides (e.g., 37 ± 2 kJ mol^{-1} between two chair forms for 2-methoxy-1,3-dimethylhexahydropyrimidine[8a]). Hence, the relative orientation of the 2′-OH group in the pentofuranose moiety, which is pseudoaxial in the north-form and pseudoequatorial in the south-form (Figure 1), should dictate its solvation pattern as well as its intramolecular interaction. Interestingly, this flexible nature of the hydroxyl orientation in 2′-OH (i.e., $\Phi_{H2'-C2'-O2'-H}$) and/or 3′-OH (i.e., $\Phi_{H3'-C3'-O3'-H}$) depending on the conformationally labile pentose sugar geometry poses problems in our attempts to understand the nature of the H-bonding in the furanose compared to the pyranose system, and, in fact, this is the first experimentally based (NMR) report describing an insight into this problem.

Results and Discussion

To understand the chemical uniqueness of the 2′-OH group vicinal to a 3′-phosphodiester function in RNA, we have undertaken a study of adenosine 3′-ethyl phosphate (**1**), which is the most simple phosphodiester model system mimicking that of a monomeric unit of RNA, and because of the simplicity of the model, it should be possible to understand the chemical nature of the constituent 2′-OH group in greater detail. Clearly, this is possible only by a comparative study involving both adenosine (**3**) and 3′-deoxyadenosine (**2**).

The culmination of at least four different competing effects determines the δ_{OH} in **1**−**3**: (i) the substituent

(2) (a) Acharya, P.; Trifonova, A.; Thibaudeau, C.; Földesi, A.; Chattopadhyaya, J. *Angew. Chem., Int. Ed. Engl.* **1999**, *38*, 3645. (b) Velikyan, I.; Acharya, S.; Trifonova, A.; Földesi, A.; Chattopadhyaya, J. *J. Am. Chem. Soc.* **2001**, *123*, 2893. (c) Gellman, S. H.; Dado, G. P.; Liang, G.; Adams, B. R. *J. Am. Chem. Soc.* **1991**, *113*, 1164 and references therein. (d) Winningham, M. J.; Sogah, D. Y. *J. Am. Chem. Soc.* **1994**, *116*, 11173. (e) Stevens, E. S.; Sugawara, N.; Bonora, G. M.; Toniolo, G. *J. Am. Chem. Soc.* **1980**, *102*, 7048. (f) Harris, T. K.; Mildvan, A. S. *PROTEINS: Structure, Function, Genet.* **1999**, *35*, 275.

(3) Fraser, R. R.; Kaufman, M.; Morand, P.; Govil, G. *Can. J. Chem.* **1969**, *47*, 403.

(4) (a) St-Jacques, M.; Sundararajan, P. R.; Taylor, K. J.; Marchessault, R. H. *J. Am. Chem. Soc.* **1976**, *98*, 4386. (b) Bernet, B.; Vasella, A. *Helv. Chim. Acta* **2000**, *83*, 995 and references therein. (c) Sandström C.; Baumann, H.; Kenne, L. *J. Chem. Soc., Perkin Trans. 2* **1998**, 2385.

(5) The two-state dynamic N ⇆ S pseudorotational equilibrium in nucleosides was based on statistical distributions of X-ray crystal structures (ref 5d) and the solution NMR observations as evident by their respective chemical shifts and $^3J_{H,\,H}$ of the constituent sugar moieties in oligonucleotides as in B ⇆ Z DNA (ref 5a) or A ⇆ Z RNA (ref 5b) or in the A-form ⇆ B-form lariat RNA (ref 5c): (a) Feigon, J.; Wang, A. H.-J.; van der Marel, G. A.; van Boom, J. H.; Rich, A. *Nucleic Acids Res.* **1984**, *12*, 1243. (b) Davis, P. W.; Hall, K.; Cruz, P.; Tinoco, I., Jr.; Neilson, T. *Nucleic Acids Res.* **1986**, *14*, 1279. (c) Agback, P.; Sandström, A.; Yamakage, S.-i.; Sund, C.; Glemarec, C.; Chattopadhyaya, J. *J. Biochem. Biophys. Methods* **1993**, *27*, 229. (d) de Leeuw, H. P. M.; Haasnoot, C. A. G.; Altona, C. *Isr. J. Chem.* **1980**, *20*, 108. (e) Saenger, W. *Principles of Nucleic Acid Structure*; Springer-Verlag: Berlin, 1988.

effect, (ii) the intramolecular H-bonding effect, (iii) the solvation and the nature of the solvent, and (iv) the conformation of the pentose sugar and consequently the conformation-dependent orientation of the hydroxyl group. The 3′-substituent effect on the intramolecular H-bonding of 2′-OH in **1** and **3**, compared to **2**, can be conveniently determined in DMSO-d_6, since the chemical shift of hydroxyl protons (δ_{OH}) in DMSO-d_6 is strongly dependent not only on H-bonding or metal ion binding but also on subtle structural effects in nucleos(t)ides that act directly and/or indirectly on the electronic environment of the OH groups. Thus, the chemical shifts of 2′-OH in **1**−**3** are as follows: $\delta_{2'-OH}$ = 7.305 ppm in **1,** 5.484 ppm in **2**, and 5.365 ppm in **3** at 298 K [compare also $\delta_{3'-OH}$ in **3** (5.106 ppm) with that of 2′-deoxyadenosine (5.246 ppm)[9c]]. Thus, the pairwise comparison of $\delta_{2'-OH}$ in 3′-deoxyadenosine and adenosine, on one hand, and $\delta_{3'-OH}$ in 2′-deoxyadenosine and adenosine, on the other hand, shows the effects of both inter- and intramolecular H-bonding and the stereoelectronic effects.[6n,7a]

Since the hydroxyl groups in nucleosides can take up different pseudoaxial or pseudoequatorial orientations[5,6a,b,7] depending upon the sugar conformation, it was necessary to understand which conformation is predominant for **1**−**3** over the temperature range studied. Thus, the sugar conformations for adenosine 3′-ethyl phosphate (**1**) and adenosine (**3**) are found to be predominantly S-type (the population of the S-type pseudorotamers at 288 and 368 K are, respectively, 85% and 73% for **1**, 71% and 60% for **3**), whereas for 3′-deoxyadenosine (**2**) it is found to be predominantly the N-type [71% N (288 K) and 65% N (368 K)] over the whole temperature range in DMSO-d_6 (Figure 1). This suggests that the sugar pucker should be fixed in the same conformation as that of the major NMR conformer for performing NMR constrained molecular modeling of the hydroxyl orientation in order to understand the intrinsic hydrogen-bonding process.

We here report (i) the orientation of 2′-OH proton by detailed exocyclic ($^3J_{H,OH}$) coupling constant analyses in conjunction with the concentration as well as solvent polarity dependent studies. (ii) The temperature-dependent line-shape analysis of the hydroxyl protons studies has enabled us to thermodynamically assess intramolecular 2′O−H···O3′ H-bonding process in **1** and **3** in comparison with **2**. (iii) The hydration of the 2′-O−H··· O3′−H(phos) system in our model RNA system, adenosine 3′-ethyl phosphate (**1**), in comparison with that of adenosine (**3**) in DMSO- d_6 have also allowed us to measure the exchange rate of this hydrogen-bonded 2′-OH with bound water in order to understand the role of hydration of 2′-OH in the RNA-folding process.

That the DMSO-d_6 as a solvent actually mimics the aqueous solution environment of nucleosides and nucleotides in terms of the nature of H-bonding is evident from four different NMR observations: (i) Among **1**−**3**, the intramolecularly H-bonded nature of the 2′-OH in adenosine 3′-ethyl phosphate (**1**)[6d] is directly evident by the 16-line multiplicity of the nonequivalent methylene protons in the ethyl phosphate moiety (<338 K). Similar nonisochronacity of the methylene protons of the 3′-ethyl phosphate moiety in adenosine 3′-ethyl phosphate (**1**) has been found in DMSO-d_6 as in aqueous solution.[6d,7a] (ii) The ΔG^{H-bond}_{298K} calculated from the line-shape analysis of this methylene protons splitting in **1** are comparable (Table 6) both in aqueous and DMSO-d_6 solutions. (iii) Similar sugar pucker population as well as the geometry of the constituent pentose ring in **1**−**3** have been found in both water[6a−d,7a] and DMSO-d_6 (see the Experimental Section for details). (iv) Finally, the shells of hydration around the hydroxyl groups of **1** and **3** have been found at the water resonance at ∼3.286 ppm in the NOESY and ROESY experiments over 308−348 K.

(6) (a) Koole, L. H.; Buck, H. M.; Bazin, H.; Chattopadhyaya, J. *Tetrahedron* **1987**, *43*, 2989. (b) Koole, L. H.; Buck, H. M.; Nyilas, A.; Chattopadhyaya, J. *Can J. Chem.* **1987**, *65*, 2089. (c) Plavec, J.; Tong, W.; Chattopadhyaya, J. *J. Am. Chem. Soc.* **1993**, *115*, 9734. (d) Plavec, J.; Thibaudeau, C.; Viswanadham, G.; Sund, C.; Sandström A.; Chattopadhyaya, J. *Tetrahedron* **1995**, *51*, 11775. (e) Plavec, J.; Thibaudeau, C.; Chattopadhyaya, J. *J. Am. Chem. Soc.* **1994**, *116*, 6558. (f) Plavec, J.; Thibaudeau, C.; Viswanadham, G.; Sund, C.; Chattopadhyaya, J. *J. Chem. Soc. Chem. Commun.* **1994**, 781. (g) Thibaudeau, C.; Plavec, J.; Garg, N.; Papchikhin, A.; Chattopadhyaya, J. *J. Am. Chem. Soc.* **1994**, *116*, 4038. (h) Thibaudeau, C.; Plavec, J.; Chattopadhyaya, J. *J. Org. Chem.* **1996**, *61*, 266. (i) Plavec, J.; Thibaudeau, C.; Chattopadhyaya, J. *Pure Appl. Chem.* **1996**, *68*, 2137. (j) Thibaudeau, C.; Földesi, A.; Chattopadhyaya, J. *Tetrahedron* **1997**, *53*, 14043. (k) Luyten, I.; Thibaudeau, C.; Chattopadhyaya, J. *J. Org. Chem.* **1997**, *62*, 8800. (l) Luyten, I.; Thibaudeau, C.; Chattopadhyaya, J. *Tetrahedron* **1997**, *53*, 6433. (m) Thibaudeau, C.; Plavec, J.; Chattopadhyaya, J. *J. Org. Chem.* **1997**, *62*, 8800. (n) The stereoelectronic O3′−C3′−C4′−O4′ *gauche* effect[2a,6a−d,h,i,m,7a] (3′-GE) will reduce the electron density at C3′ because of charge transfer from σ orbital of C3′−H3′ ($\sigma_{C3'-H3'}$) to the antibonding orbital of C4′−O4′ (i.e., $\sigma_{C3'-H3'} \rightarrow \sigma^*_{C4'-O4'}$ orbital mixing) which can only take place in the S-type conformation[2a,6g,7a] giving an overall deshielding of 3′-OH. Since the population of S-type conformation of pentose-sugar in adenosine (vide infra) is relatively less than that of 2′-deoxyadenosine (Table S9 in the Supporting Information), the GE is more predominant in the latter than in the former (since 3′-GE works only in S-type conformation[6g]), thereby explaining why the 3′-OH in 2′-deoxyadenosine is shifted more downfield compared to that of adenosine. Similarly, stereoelectronic O2′−C2′−C1′−O4′ gauche effect (2′-GE, i.e., $\sigma_{C2'-H2'} \rightarrow \sigma^*_{C1'-O4'}$ orbital mixing)[6a−c,e,7a] and O4′−C1′−N9 anomeric effect (AE, i.e., $n_{O4'} \rightarrow \sigma^*_{C1'-N9}$ orbital mixing)[6h,i,m,7a] are favored in the N-type conformation in 3′-deoxyadenosine, which drive the pentose sugar to the preferred N-type conformation (vide infra). In contrast, competing 3′-GE weakens 2′-GE and AE in adenosine[6i,7a] which results in the shift of the sugar conformation predominantly to the S-type (vide infra). This explains why $\delta_{2'-OH}$ in 3′-deoxyadenosine is more downfield compared to that in adenosine. This stereoelectronic argument can be further strengthened by examining the pK_a of 2′-OH and 3′-OH groups.[2b] *Note that these secondary hydroxyl groups of the pentose sugar moiety[2b] are found to be more acidic than any other alicylic or aliphatic secondary alcohols by ca. 2 orders of magnitude, owing to intrinsic stereoelectronic structural makeup of the pentose sugar.*[7a] Thus the pK_a for 3′-OH of 2′-deoxyadenosine is found to be 13.02 ± 0.03 from pH dependent δH3′, compared to the pK_a of 2′-OH of 3′-deoxyadenosine (12.65 ± 0.05 from pH-dependent δH2′).[2b] The reason for the latter to be slightly more acidic than the former lies in the fact that the 3′-oxyanion in S-type conformation in 2′-deoxyadenosine is stabilized by single 3′-GE, whereas the 2′-oxyanion in 3′-deoxyadenosine with preferred N-type sugar is stabilized by at least two different stereoelectronic effects: the 2′-GE as well as by AE (which are slightly opposed by O2′−N9 gauche effect).

(7) (a) For a review, see: Thibaudeau, C.; Chattopadhyaya, J. *Stereoelectronic Effects in Nucleosides and Nucleotides and their Structural Implications*, (ISBN 91-506-1351-0), Department of Bioorganic Chemistry, Uppsala University Press (fax: +4618554495), Sweden, 1999 and references therein. (b) Kilpatrick, J. E.; Pitzer, K. S.; Spitzer, R. *J. Am. Chem. Soc.* **1947**, *64*, 2483.

(8) (a) Perrin, C. L.; Armstrong, K. B.; Fabian, M. A. *J. Am. Chem. Soc.* **1994**, *116*, 715. (b) Röder, O.; Lüdemann, H.-D.; von Goldammer, E. *Eur. J. Biochem.* **1975**, *53*, 517.

(9) (a) West, R. T.; Garza, L. A., II; Winchester, W. R.; Walmsley, J. A. *Nucl. Acid Res.* **1994**, *22*, 5128. (b) The PDB structures of our NMR constrained molecular modeling studies have shown that for **2**, the distance between N3 and 2′-OH ($d_{N3\cdots HO2'}$) is 5.48, 4.45, and 4.5 Å as well as that between O4′ and 2′-OH ($d_{O4'\cdots HO2'}$) is 3.94, 3.71, and 3.1 Å at energy minimised $\Phi_{H2'-C2'-O2'-H}$ of 45.2°, −45.2° and −124.0°, respectively. (c) The similar NMR studies in DMSO-d_6 as well as NMR constrained molecular modeling studies have been performed for 2′-deoxyadenosine (**4**). $\delta_{3'-OH}$ and $\delta_{5'-OH}$ for **4** are found to be 5.246 and 5.167 ppm at 298 K. The NMR constrained molecular modeling for **4** has shown a broad minimum of $-121.4° \leq \Phi_{H3'-C3'-O3'-H} \leq 121.4°$ which indicates a free rotor for 3′-OH in that torsional hyperspace, since no intramolecular interaction is possible like in **2**. However the minima for $\Phi_{H3'-C3'-O3'-H}$ is more spreaded compared to that in **2** as the hydroxyl is away from the aglycon.

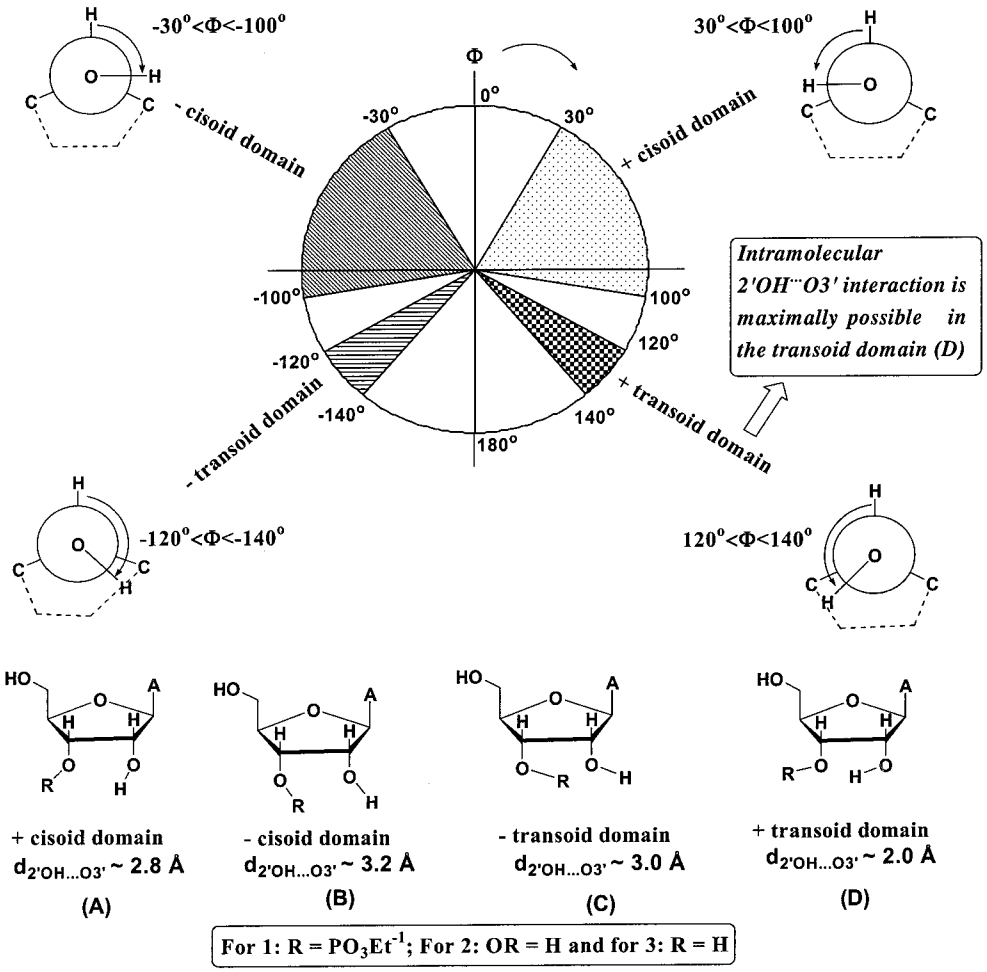

Figure 2. Torsional hyperspace for both $\Phi_{H2'-C2'-O2'-H}$ (Φ_1) and $\Phi_{H3'-C3'-O3'-H}$ (Φ_2) represented in the wheel by Φ. The relative orientations of the Φ_1 and Φ_2 are shown in the chemical formulas below. The Φ_1 and Φ_2 have been calculated from temperature-dependent $^3J_{H2',OH}$ and $^3J_{H3',OH}$, respectively (Table 1) using the Karplus equation $^3J_{H,OH} = 10.4 \cos^2 \Phi - 1.5 \cos \Phi + 0.2$[3] for adenosine 3′-ethyl phosphate (**1**), 3′-deoxyadenosine (**2**), and adenosine (**3**). The possible solutions of the Karplus equation[3] using NMR-derived $^3J_{H,OH}$ (Table 1) show four major domains in the torsional hyperspace for $\Phi_{H,OH}$ viz. (A) positive cisoid domain (from 30° to 100°); (B) negative cisoid domain (from −30° to −100°); (C) negative transoid domain (from −120° to −140°), and (D) positive transoid domain (from 120° to 140°). The relative proximities of the 2′- and 3′-OH (average value of $d_{2'OH\cdots O3'}$ in Å as found from molecular model building) at those different combinations (A−D) of the torsional orientations are also shown.

(A) Comparison of Orientations of the 2′- and 3′-OH Proton by $^3J_{H2',OH}$ and $^3J_{H3',OH}$ Analysis. The $^3J_{H2',OH}$ coupling constants for adenosine 3′-ethyl phosphate (**1**), 3′-deoxyadenosine (**2**), and adenosine (**3**) at 298 K are as follows: 4.1 Hz for **1**, 4.3 Hz for **2**, and 6.1 Hz for **3**. Similarly, $^3J_{H3',OH}$ of 4.5 Hz has been found for **3** at 298 K. According to Karplus equation,[3] four dihedral solutions, two in the cisoid (± 30° to ± 80°) and two in the transoid (± 120° to ± 150°, Figure 2) domains, are possible for each of the $^3J_{H2',OH}$ (i.e., for $\Phi_{H2'-C2'-O2'-H}$) and $^3J_{H3',OH}$ (i.e., for $\Phi_{H3'-C3'-O3'-H}$). The $\Phi_{H2'-C2'-O2'-H}$ of the pseudoequatorial 2′-OH (2′-OH_{peq}) with S-type sugar conformation in positive transoid domain corresponds to the closer proximity to the neighboring O3′ (Figure 2). In DMSO-d_6, fully solvated equatorial and axial OH group in pyranosides are characterized by $^3J_{H,OH}$ values between 4.2 and 5.7 Hz for the former and between 3.0 and 4.2 Hz for the latter.[4b]

(i) The Nature of 2′-OH in Adenosine 3′-Ethyl Phosphate (1) and 3′-Deoxyadenosine (2). The earlier NMR studies[6d] of adenosine 3′-ethyl phosphate (**1**) in D_2O[6d] (as well as here in DMSO-d_6) revealed the existence of nonequivalent methylene protons [16 line multiplicity arising from the $^3J_{H,P}$, $^3J_{H,H}$, and $^2J_{H,H}$ viz. (2 × 2 × 2) + (2 × 2 × 2) for two nonequivalent methylene protons] of the 3′-ethyl phosphate group in the (S,ε^-) state[6d] at low temperature, which disappears at high temperature (>348 K) resembling those of the isochronous methylene protons of the 2′-deoxy counterpart.[6d] This temperature-dependent phenomenon in **1** has been attributed to different electronic (chemical) environments around the methylene protons due to the presence of the intramolecular H-bonding [2′-OH···O3′] at low temperature.

Although adenosine 3′-ethyl phosphate (**1**) (in S-type) and 3′-deoxyadenosine (**2**) (in N-type) have very similar $^3J_{H2',OH}$ (4.2−4.3 Hz), the NMR-constrained molecular modeling studies (Table 2 and Figure 3) have shown very different torsional angles of their respective 2′-OH (i.e., $\Phi_{H2'-C2'-O2'-H}$). Thus, the torsional hyperspace scan (Figure 2) by NMR-constrained geometry optimizations with AM1,[14a] PM3, as well as ab initio gas-phase HF/Midi![12] calculations using the Gaussian 98 program and solution-phase (ε = 46.5 at 298 K) HF/6-31+G*//HF/Midi! calculations[12] (Table 2 and Figure 3A) have shown that the $^3J_{H2',OH}$ of 4.1 Hz (298 K) for **1** characterizes the lowest

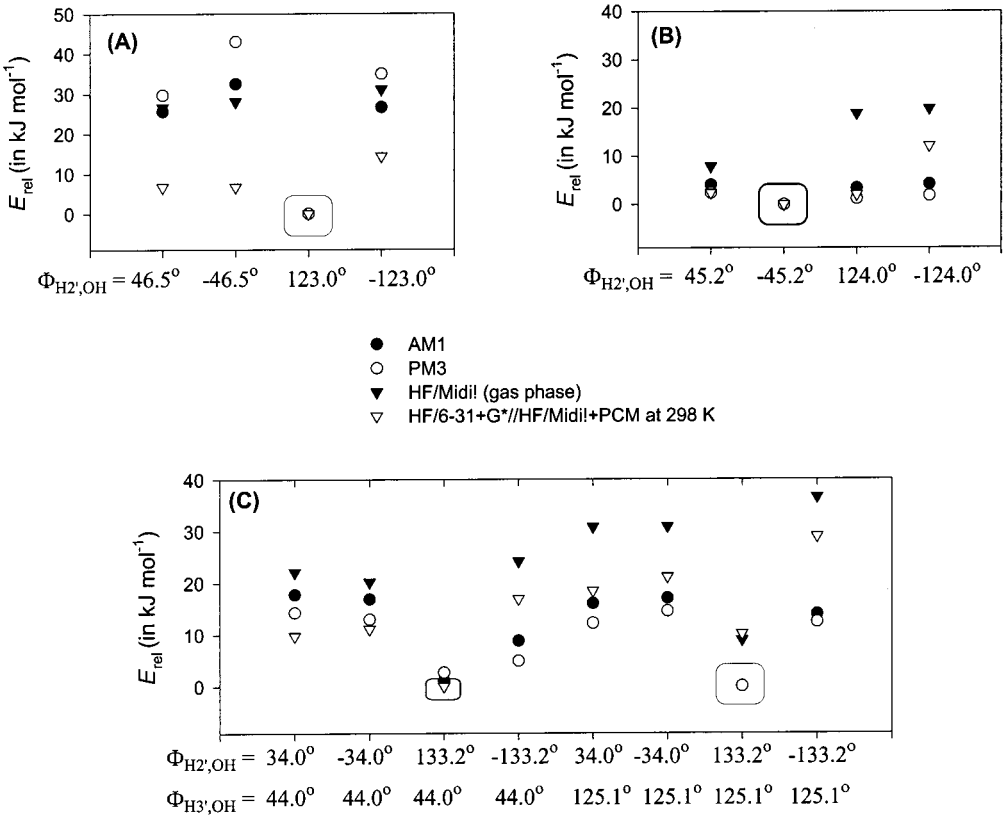

Figure 3. Panels A−C represent the plot of relative energy [E_{rel}, in kJ mol^{-1}, see Table 2 for details] as a function of $\Phi_{H,OH}$ for adenosine 3′-ethyl phosphate (**1**), 3′-deoxyadenosine (**2**), and adenosine (**3**) (i.e., $\Phi_{H2',OH}$ for **1** and **2**, whereas both $\Phi_{H2',OH}$ and $\Phi_{H3',OH}$ for **3**, see Table 1). Geometry optimizations (see Table 2 and the Experimental Section for details) have been performed by NMR-constrained semiempirical AM1[14a] (●), PM3 (○), and ab initio gas-phase HF/Midi! (▼) as well as solution phase (ε = 46.5 using PCM solvation model at 298 K) HF/6-31+G*//HF/Midi! (▽). Both semiempirical and ab initio calculations (in gas and solution phase) predict the energy minimum of $\Phi_{H2',OH}$ is at 123.5° in **1** (panel A)]and $\Phi_{H2',OH}$ at −45.2° for **2** (panel B). However, for **3** (panel C), the semiempirical calculation indicates the energy minima of $\Phi_{H2',OH}$ and $\Phi_{H3',OH}$ are at 133.2° and 125.1°, respectively, whereas ab initio calculations predict the minima of $\Phi_{H2',OH}$ and $\Phi_{H3',OH}$ are at 133.2° and 44.0°, respectively. The box in each graph shows the global energy minimum (E_{rel} = 0 kJ mol^{-1}) of the corresponding $\Phi_{H,OH}$.

energy minimum of $\Phi_{H2'-C2'-O2'-H}$ in the positive transoid region (123.0°) (i.e., proximity toward O3′, Figure 2). This further corroborates that the 2′-OH in **1** is clearly the proton donor for intramolecular H-bonding with the vicinal O3′ (i.e., the bridging oxygen of the vicinal 3′-phosphate), which is also consistent with earlier molecular mechanics studies.[6d] An alternate possibility of intramolecular H-bonding between 2′-OH and the vicinal nonbridging phosphoryl oxygens [2′-OH···phosphate−oxygen] in **1** has been ruled out by ab initio calculations (at HF/Midi! level[12]). This study clearly shows that, at the global energy minimum, the closest distance from 2′-OH to any of the nonbridging phosphoryl oxygens is at least 3−4 Å, which indicates that it is simply not possible to form a H-bond between them. This observation is also

(10) (a) Hruby, V. J. In *Chemistry and Biochemistry of Amino Acids, Peptides and Proteins*; Weinstein, B., Ed.; M. Dekker Inc.: New York, 1974; Vol. 3, p 14. (b) Scheiner, S. In *Reviews in Computational Chemistry*; Lipkowitz, K. B., Boyd, D. B., Eds.; VCH Publishers Inc.: New York, 1991; Vol. 2, p 165. (c) Lommerse, J. P. M.; Price, S. L.; Taylor, R. *J. Comput. Chem.* **1997**, *18*, 757. (d) Schmiedekamp-Schneeweis, L. A.; Payne, J. O. *Int. J. Quantum Chem.* **1998**, *70*, 863. (e) Bene, J. E. D.; Perera, S. A.; Barlett, R. J. *J. Phys. Chem. A* **1999**, *103*, 8121. (f) Kumar, G. A.; McAllister, M. A. *J. Org. Chem.* **1998**, *63*, 6968.

(11) (a) Birnbaum, G. I.; Giziewicz, J.; Huber, C. P.; Shugar, D. *J. Am. Chem. Soc.* **1976**, *98*, 4640 and references therein. (b) Bolton, P. H.; Kearns, D. R. *J. Am. Chem. Soc.* **1979**, *101*, 479. (c) Markley, J. L.; Westler, W. M. *Biochemistry*, **1996**, *35*, 11092. (d) Lin J.; Frey P. A. *J. Am. Chem. Soc.* **2000**, *122*, 11258. (e) Maltseva, T. V.; Agback, P.; Chattopadhyaya, J. *Nucleic Acid Research*, **1993**, *21*, 4246 and references therein. (f) Maltseva, T. V.; Chattopadhyaya, J. *Tetrahedron* **1995**, *51*, 5501.

(12) Frisch, M. J.; Trucks, G. W.; Schlegel, H. B.; Scuseria, G. E.; Robb, M. A.; Cheeseman, J. R.; Zakrzewski, V. G.; Montgomery, J. A., Jr.; Stratmann, R. E.; Burant, J. C.; Dapprich, S.; Millam, J. M.; Daniels, A. D.; Kudin, K. N.; Strain, M. C.; Farkas, O.; Tomasi, J.; Barone, V.; Cossi, M.; Cammi, R.; Mennucci, B.; Pomelli, C.; Adamo, C.; Clifford, S.; Ochterski, J.; Petersson, G. A.; Ayala, P. Y.; Cui, Q.; Morokuma, K.; Malick, D. K.; Rabuck, A. D.; Raghavachari, K.; Foresman, J. B.; Cioslowski, J.; Ortiz, J. V.; Stefanov, B. B.; Liu, G.; Liashenko, A.; Piskorz, P.; Komaromi, I.; Gomperts, R.; Martin, R. L.; Fox, D. J.; Keith, T.; Al-Laham, M. A.; Peng, C. Y.; Nanayakkara, A.; Gonzalez, C.; Challacombe, M.; Gill, P. M. W.; Johnson, B. G.; Chen, W.; Wong, M. W.; Andres, J. L.; Head-Gordon, M.; Replogle, E. S.; Pople, J. A. *Gaussian 98*, revision A.6; Gaussian, Inc.: Pittsburgh, PA, 1998.

(13) Strong H-bonds are highly directional involving linear arrangement of the donor and acceptor atoms. Ab initio calculations showed that in water and HF dimer[10b,e] (H-bond strength of ∼ 4−5 kcal mol^{-1}) the reported ∠X−H···X (where X = O, F respectively) are found to be ∼176° and ∼170°, respectively, and H···O distance is ∼1.0 Å. The amide−amide intramolecular H-bonding in peptides is strongest when the ∠N−H···O approaches linearity with optimum values calculated to be ∼160° and the N···O distance of ∼2.9 Å,[2a] whereas commonly reported O−H···O angle in the strong intermolecular H-bonding (H-bond strength of ∼5 kcal mol^{-1}) involving alkanol with ether and carbonyl compounds is ∼165° with O···H distance between 1.8 and 2.0 Å.[10c] However, nonlinear intramolecular H-bonds are relatively weaker due to the deviation from coplanarity between the donor and acceptor as found in resonance stabilized system like 3-substituted-2-methoxybenzoic acids[10d] and in conformationally constrained ginkgolides[4b] where ∠O−H···O and O···H distance are calculated to be ∼140° and ∼1.8 Å, respectively.

Table 1. Temperature-Dependent $^3J_{H,OH}$ Coupling Constants Involving 2′-OH and 3′-OH and Respective $\Phi_{H2'-C2'-O2'-H}$ (Φ_1 and $\Phi_{1'}$) and $\Phi_{H3'-C3'-O3'-H}$ (Φ_2 and $\Phi_{2'}$) Torsion Angles[a] for Adenosine 3′-Ethyl Phosphate (1), 3′-Deoxyadenosine (2), and Adenosine (3) in DMSO-d_6

	1			2			3					
T (K)	$^3J_{H2',OH}$	Φ_1	$\Phi_{1'}$	$^3J_{H2',OH}$	Φ_1	$\Phi_{1'}$	$^3J_{H2',OH}$	Φ_1	$\Phi_{1'}$	$^3J_{H3',OH}$	Φ_2	$\Phi_{2'}$
288	4.2	±45.9	±123.5	4.3	±45.2	±124.0	6.1	±34.0	±133.2	4.5	±44.0	±125.1
298	4.1	±46.5	±123.0	4.3	±45.2	±124.0	6.1	±34.0	±133.2	4.5	±44.0	±125.1
368	0.8	±71.2	±100.3	3.6	±49.6	±120.3	1.0	±70.0	±102.4	0.4	±76.8	±94.8

[a] The four possible solutions of torsion angles [Φ (where $\Phi = \Phi_i$, with $i = 1, 1', 2$, and $2'$) in degrees, see Figure 2] have been calculated using the Karplus equation $^3J_{H,OH} = 10.4 \cos^2 \Phi - 1.5 \cos \Phi + 0.2$.[3] Only $^3J_{H,OH}$ at the three representative temperatures (288, 298, and 368 K) have been shown.

Table 2. Torsional Hyperspace Scan of Hydroxyl Orientation in Adenosine 3′-Ethyl Phosphate (1), 3′-Deoxyadenosine (2), and Adenosine (3) from the Energy-Minimized $\Phi_{H2',OH}$ and $\Phi_{H3',OH}$ (in degrees) by NMR Constrained Geometry Optimization with Semi-Empirical as Well as ab Initio Methods Using Gaussian 98[12]

			AM1[b,c]	PM3[b,c]	HF/Midi! (gas phase)[b,c]	HF/6-31+G*//HF/Midi! (solution phase)[b,c]
compd	$\Phi_{H2',OH}$[a]	$\Phi_{H3',OH}$[a]	E_{rel}	E_{rel}	E_{rel}	E_{rel}
1	46.5		25.6	29.7	26.6	11.9
	−46.5		32.5	43.0	28.0	11.9
	123.0		**0.0**	**0.0**	**0.0**	**0.0**
	−123.0		26.6	34.9	31.0	14.3
2	45.2		4.1	2.4	7.9	2.4
	−45.2		**0.0**	**0.0**	**0.0**	**0.0**
	124.0		3.4	1.2	18.8	2.0
	−124.0		4.2	1.8	19.8	12.1
3	34.0	44.0	17.8	14.3	22.1	12.4
	−34.0	44.0	16.9	13.0	20.2	11.1
	133.2	44.0	1.1	2.7	**0.0**	**0.0**
	−133.2	44.0	8.8	4.9	24.1	16.9
	34.0	125.1	16.0	12.2	30.7	18.4
	−34.0	125.1	17.0	14.5	30.8	21.1
	133.2	125.1	**0.0**	**0.0**	8.9	9.1
	−133.2	125.1	13.9	12.4	36.5	28.9

[a] The $\Phi_{H2',OH}$ and $\Phi_{H3',OH}$ (in degrees) correspond to the solutions of the Karplus equation[3] involving $^3J_{H2',OH}$ and $^3J_{H3',OH}$ at 298 K (see Table 1). [b] In each calculation, the respective solution of $\Phi_{H2',OH}$ and $\Phi_{H3',OH}$ using the Karplus equation[3] for the corresponding $^3J_{H2',OH}$ and $^3J_{H3',OH}$ along with PSEUROT analyzed major sugar puckers for **1**−**3** were kept fixed, and the rest of the geometry was optimized freely to find the orientation of $\Phi_{H,OH}$ at global minima (see the Experimental Section for details). [c] E_{rel} are given in kJ mol^{-1}, taking consideration of the lowest energy (E_{SCF}, in Hartree atom^{-1}, see Tables S10−S15 in the Supporting Information for details) conformer as 0.0 kJ mol^{-1} and subtracting rest from that. The shaded rows represent the global energy minima corresponding to the $E_{rel} = 0$ kJ mol^{-1}, marked with a square box in Figure 3.

consistent with earlier molecular dynamics simulations[1m] of the crystal data for tRNA^{Asp} anticodon loop, which showed that the preferred orientation of 2′-OH is indeed toward O3′ in the $C_{2'}$-*endo* sugar conformation, not toward any of the nonbridging phosphate oxygens.

The NMR-constrained ($^3J_{H2',OH}$ = 4.3 Hz) potential torsional hyperspace scans with AM1[14a] and PM3 calculations for 3′-deoxyadenosine, on the other hand, have shown (Table 2 and Figure 3B) that among the four possible dihedral angles, ±124.0° or ±45.2°, the preferred energy minimum in fact lies in the range $-124.0° \leq \Phi_{H2'-C2'-O2'-H} \leq 45.2°$ for 3′-deoxyadenosine. However, the gas-phase ab initio calculation with HF/Midi! indicates a global minimum at −45.2° and a local minimum at 45.2° (having 7.9 kJ mol^{-1} energy penalty), and solution-phase HF/6-31+G*//HF/Midi! shows the preferred energy minimum between $-45.0° \leq \Phi_{H2'-C2'-O2'-H} \leq 124.0°$ for 3′-deoxyadenosine.[9b,c]

(ii) The Nature of 2′-OH in Adenosine (3). The donor−acceptor characteristic of the intramolecular H-bonding is, however, much less obvious for adenosine, which has been previously assumed to exist in either 3′-O−H···O2′ or 2′-O−H···O3′ form, mainly owing to pK_a reasons,[11a] without any rigorous experimental basis such as the $^3J_{H2'(3'),OH2'(3')}$-derived torsion of the hydroxyl groups as described here.

The existence of weak long-range $^4J_{H2',OH3'}$ in adenosine (i.e., W conformation of H2′−C2′−C3′−O3′−H) indicates the nonplausibility of the negative values for $\Phi_{H3'-C3'-O3'-H}$. Hence, among all possible Karplus[3]-derived solutions of $\Phi_{H3'-C3'-O3'-H}$ corresponding to $^3J_{H3',OH}$ of 4.5 Hz (298 K) in adenosine, the torsional values in negative cisoid and transoid domains (Figure 2) were neglected in the NMR-constrained torsional hyperspace scan. AM1[14a] and PM3 calculations have shown the global energy minimum of the $\Phi_{H2'-C2'-O2'-H}$ torsion at 133.2° (i.e., the 2′-OH turning at C3′ has a lower energy penalty in contrast with that of 3′-deoxyadenosine), whereas that for $\Phi_{H3'-C3'-O3'-H}$ torsion is found at 44° and a local minimum at 125.1° (having ∼1−3 kJ mol^{-1} energy penalty, see Table 2 and Figure 3C). Similarly, the gas and solution phase (ε = 46.5 at 298 K) ab initio calculations of adenosine with HF/Midi! and HF/6-31+G*//HF/Midi! also show the global energy minimum for $\Phi_{H2'-C2'-O2'-H}$ and $\Phi_{H3'-C3'-O3'-H}$ at 133.2° and 44°, respectively, with a local minimum for $\Phi_{H3'-C3'-O3'-H}$ at 125.1° (∼9 kJ mol^{-1} energy penalty, see Table 2 and Figure 3C), *thereby showing H-bond-accepting 3′-OH is less restricted than that of H-bond-donating 2′-OH*. This is also supported by temperature-dependent ^{1}H NMR studies, which showed that the 3′-OH is exchanged (line broadening at 343 K) relatively faster than the 2′-OH (line broadening at 353 K) in adenosine, indicating the latter being involved as the proton donor in the intramolecular H-bonding in adenosine rather than the former (i.e., 2′-O−H···O3′). This is further supported by evidence based on the solvent polarity studies;[14a] nevertheless, the widely used temperature coefficient ($\Delta\delta/\Delta T$) study[14b] of the hydroxyl chemical shift in our systems

could not yield any direct evidence regarding intramolecular H-bonding.[14a,b]

(a) Concentration-Dependent Studies. Except the hydroxyl protons in adenosine 3′-ethyl phosphate (**1**) ($[\Delta\delta_{2'-OH}]_{\Delta concd} = 0.357$ ppm and $[\Delta\delta_{5'-OH}]_{\Delta concd} = 0.09$ ppm) the chemical shifts for all other hydroxyl protons in 3′-deoxyadenosine (**2**) and adenosine (**3**) show relatively small change (<0.1 ppm) as a function of concentration (5−200 mM), thereby showing that, besides the intramolecular H-bonding in **1** and **3**, the self-aggregation process in **1** is more dominant than in **2** and **3**.

(b) Solvent Polarity Studies.[14a] Both polarity and the intermolecular H-bonding capacity of the solvent influence the conformation and the strength of the intramolecular H-bonding for hydroxyl protons.[2a] Since the H-bond is electrostatic in nature[2c,4a] the polarity of the solvent is indeed a dominant factor. With the slow addition of D_2O in the DMSO-d_6 solution of **3** the change of δ_{OH} ($\Delta\delta_{2'-OH} = 0.024$ ppm < $\Delta\delta_{3'-OH} = 0.031$ ppm < $\Delta\delta_{5'-OH} = 0.040$ ppm) shows relatively poorer accessibility of water molecule toward 2′- and 3′-OH compared to the 5′ counterpart, owing to the presence of 2′-O−H···O3′ intramolecular H-bonding. Based on the $^3J_{H,OH}$-derived torsional flexibility, we have argued (vide infra) that 2′-OH is indeed the proton donor compared to its 3′-counterpart in **3**, which is further supported by lesser $\Delta\delta_{2'-OH}$ (0.024 ppm) compared to $\Delta\delta_{3'-OH}$ (0.031 ppm) in **3**.

(B) Geometry of 2′-OH-Mediated Intramolecular H-Bond. The conformational grid search (Table 3) by molecular mechanics calculations (see the Experimental Section for details) shows that in adenosine 3′-ethyl phosphate (**1**), the closest approach of 2′-OH toward O3′ is at 2.2 Å, which corresponds to $^3J_{H2',OH}$ of 4.2 Hz at 288 K, and farthest at 2.75 Å corresponds to $^3J_{H2',OH}$ of 0.8 Hz at 368 K. Similarly, in adenosine (**3**), the closest approach of 2′-OH toward O3′ ($d_{2'OH\cdots O3'}$) at 2.25 Å corresponds to $^3J_{H2',OH}$ and $^3J_{H3',OH}$ of 6.1 and 4.5 Hz at 288 K and farthest at 2.55 Å corresponds to $^3J_{H2',OH}$ and $^3J_{H3',OH}$ of 1.0 and 0.4 Hz at 368 K. The solution phase NMR constrained ab initio calculation ($\varepsilon = 46.5$ at 298 K with HF/6-31+G*//HF/Midi!) starting from the above molecular mechanics optimized geometry shows the intramolecular $d_{2'OH\cdots O3'} = 1.97$ Å for **1** and 1.99 Å for **3** at the energy minima (Table 3). The intramolecular H-bond network between 2′- and 3′-OH is attached to the puckered sugar moiety, which expectedly causes the deviation from coplanarity along the O−H···O thereby making this nonlinear intramolecular H-bond[13] rather weaker in both nucleosides and nucleotides. At the low-energy minimum of our NMR constrained structures for both **1** and **3**, we find a rather long H-bonded bridge (∼2.2 Å with molecular mechanics and ∼2.0 Å with ab initio using Gaussian 98,[12] see Table 3) and considerably smaller ∠O−H···O3′ bond angle[13] over the temperature range studied [113.6° (288 K) ≤ ∠O−H··O3′ ≤ 93° (368 K)] with molecular mechanics and ∼120° (298 K) with ab initio calculations, see Table 3], thereby suggesting a relatively weaker 2′-OH···O3′ H-bond in both of them (in fact, our experimental $-\Delta G^{\ddagger} \cong \Delta G^{H-bond}_{298K}$ supports this conclusion: vide infra).

(C) Enthalpic vis-à-vis Entropic Effects in Intra- and Intermolecular H-Bond of 2′- and 3′-OH. The line shape analyses for 2′- and 3′-hydroxyl resonances in **1**−**3** (Figure 4) as well as that for the methylene protons of 3′-ethyl phosphate moiety in **1** have been used here to shade light on the thermodynamics of the intra- as well as the intermolecular H-bonding. The exchange rate[11b,e,f] [k^1_{ex}], [k^1_{ex} = dipole−dipole interaction + Cross-relaxation process, k^2_{ex}, vide infra], for the hydroxyl protons in **1**−**3** and methylene protons of 3′-ethyl phosphate moiety in **1** were measured from the line width at half-

Table 3. Geometrical Parameters of Intramolecular [2′-OH···O3′] H-Bond in Adenosine 3′-Ethyl Phosphate (1) and Adenosine (3) As Calculated from NMR Constrained Molecular Mechanics (MM)[a] and ab Initio[b] Calculations

	288 K		298 K		368 K	
parameters	**1**	**3**	**1**	**3**	**1**	**3**
$d_{2'OH}\cdots O3'$[c]	2.20	2.25	2.25[d] 1.973[e]	2.25[d] 1.987[e]	2.75	2.55
∠O−H···O3′[e]	113.6	113.56	112.15[d] 120.87[e]	113.56[d] 118.62[e]	92.33	92.89
EP[e]			−1.0913[f]	−0.9738[f] −0.9291[g]		

[a] Molecular Mechanics (MM) calculations have been performed using SYBYL (v. 6.2), based on the Tripos force field with conjugate gradiant method (see the Experimental Section for details). [b] NMR constrained ab initio geometry optimizations have been performed with the HF/Midi! (gas phase) and HF/6-31+G*//HF/Midi! (including PCM solvation model) basis set using Gaussian 98[12] (see Table 2 and the Experimental Section for details). [c] $d_{2'-OH}\cdots O3'$ in Å and ∠O−H···O3′ in degrees. [d] Calculated from the conformational grid search by Molecular Mechanics (MM) calculations using SYBYL (v. 6.2); see the Experimental Section for details. [e] From the energy-minimized structure of NMR-constrained solution phase (employing PCM model with $\varepsilon = 46.5$ at 298 K) ab initio HF/6-31+G*//HF/Midi! calculations using Gaussian 98.[12] [f] For 2′-O*H*. [g] For 3′-O*H*.

(14) (a) Acharya, P.; Velikian, I.; Acharya, S.; Chattopadhyaya, J. *Nucleosides, Nucleotide Nucl. Acids* **2001**, *20*, 1211. (b) Earlier $\Delta\delta/\Delta T$[2a] has been referred as a proof of the nature of the H-bonding associated with the NH group in amides[2a] and the OH group of the hexapyranose system in monosaccharides.[4b] Smaller $|\Delta\delta/\Delta T|$ indicates the internally H-bonded state, whereas larger value shows the solvent exposed state.[2b,c,4b] According to Hruby et al.[10] $\Delta\delta/\Delta T$ values of −5 to −8 ppb K^{-1} have been assigned to fully solvated OH groups of pyranoses in DMSO-d_6, and $\Delta\delta/\Delta T$ values of −1 to −2.5 ppb K^{-1} to OH groups acting as proton donors in the strong intramolecular H-bond. For all of our pentofuranose derivatives (**1**−**3**) the $\Delta\delta/\Delta T$ values for 2′-OH are very similar: [−3.8 ppb K^{-1} for **1**, −3.8 ppb K^{-1} for **2**, and −4.3 ppb K^{-1} for **3**], although the 2′-OH in **1** and **3** is pseudoequatorial in S-type sugar conformation, and in **2**, it is pseudoaxial in the N-type sugar conformation. It therefore appears that owing to the different chemical environment around the 2′-OH group in **1**−**3**, depending upon the neighboring substituents as well as the flexibile nature of the pentose ring and its conformational control on the orientation of the 2′-OH, the $\Delta\delta/\Delta T$ argument cannot be used to deduce its nature of H-bonding as in the pyranoses.[4a,b] (c) The equilibrium of *noncatalytic* exchange reaction of the H-bonded 2′-OH protons in **1** and **3** at a neutral condition where 2′-O−H···O3′-phos and 2′-O−H···O3′−H are indicative for **1** and **3** respectively. (d) This equilibrium for 2′-OH protons in **1** can be shown as [2′-O−H···O3′-(phos) + H*OD ⇆ 2′-O−H*···O3′-(phos) + 2′-O−H*···O3′-(phos) + HOD]. It is generally accepted[11e] that in case of imino proton exchange process of the base-pairing kinetics in oligonucleotides the limiting rate of exchange process (k_{ex}) is dictated by rate of opening (k_{op}) and closing (k_{cl}) of the base-pairing process which are in the nanosecond range. To extrapolate the similar situation in our case of intramolecular H-bonding we have envisioned the first step of the above-mentioned equilibrium as: closed form (2′-O−H···O3′) $\underset{k_{cl}}{\overset{k_{op}}{\rightleftharpoons}}$ open form (2′-O−H + O3′) $\xrightarrow{k_{ex}}$ exchange (2′-O−H* + O3′). The 2′-OH in adenosine (**3**) [pK_a = 12.17] is more acidic[2b] compared to that of adenosine 3′-ethyl phosphate (**1**) [pK_a = 12.68][2b]. Nevertheless, the estimated free energies for intramolecular H-bonding ($-\Delta G^{\ddagger} \cong \Delta G^{H-bond}_{298K}$, in DMSO-$d_6$ with hydration shell around hydroxyl group) in **1** and **3** are the same. This shows that the k_{op}/k_{cl} should also be same for both adenosine and its 3′-ethyl phosphate derivative. So, the lower activation energy (E_a) of exchange of 2′-OH in **1** compared to **3** has to be attributed to the more availability of the bound-water due to the presence of hydrophilic 3′-ethyl phosphate moiety in **1**. It therefore leads us to conclude that if other intra- or intermolecular interactions are possible with a potential donor or acceptor function in close spatial proximity of 2′-OH in adenosine 3′-ethyl phosphate (**1**), it may effectively compete with the bound-water.

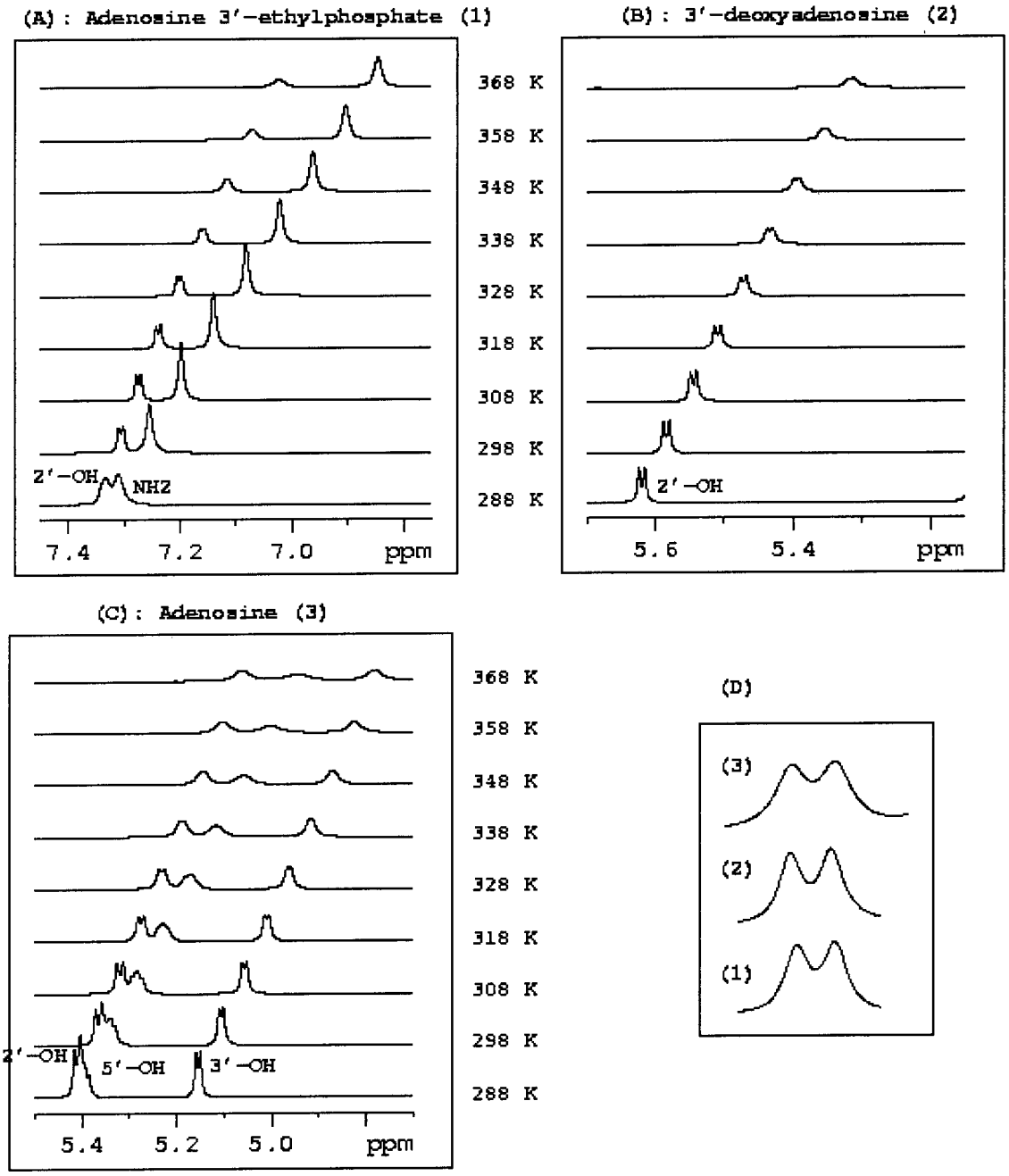

Figure 4. Panels A−C show the temperature-dependent (over the range of 288−368 K) hydroxyl resonances for adenosine 3′-ethyl phosphate (**1**), 3′-deoxyadenosine (**2**), and adenosine (**3**), respectively, in DMSO-d_6. Panel D shows the comparison of $^3J_{H2',OH}$ for **1**−**3** (4.2 Hz for **1**, 4.3 Hz for **2**, and 6.0 Hz for **3**) at 308 K.

height (halfwidth, $\Delta\nu_{1/2}$, in Hz, see Table 5) using the relation $k = \pi\Delta\nu_{1/2}$.[11b] On the basis of the reaction rate theory, the thermodynamic parameters have been calculated[11c,d] from the plot of ln k_{ex}^1 for the 2′-OH and/or 3′-OH in **1**−**3** (see Table 6 and the legend of Figure 5) as well as ln k_{ex}^1 for the methylene protons in **1**, as a function of inverse of the temperature. The free energies for exchange ($-\Delta G^{\ddagger} \cong \Delta G_{298K}^{H-bond}$ for the nonlinear intra- and intermolecular H-bonding) of the 2′- and 3′-OH in **1**−**3** (Table 6) are close to the ∼8.4 kJ mol^{-1}, which is the usual value[1a] for weak nonlinear H-bonding.[13]

The donor 2′-OH in the intramolecular H-bonding is nevertheless slightly less flexible due to the loss of conformational freedom compared to the acceptor 3′-OH, thereby showing $[-T\Delta S^{\ddagger}]_{2'-OH} < [-T\Delta S^{\ddagger}]_{3'-OH}$ in **3** [−17.9-(±0.5) kJ mol^{-1} and −19.8(±0.6) kJ mol^{-1}, respectively, at 298 K, Table 4], also supporting our donor−acceptor argument (vide infra) for the 2′-OH···O3′ intramolecular H-bonding in **3**. The entropic gain for 2′-OH in **3** compared to **1** [−15.0(±0.6) kJ mol^{-1} in **1** and −17.9-(±0.5) kJ mol^{-1} in **3** at 298 K, Table 4] is offset by the greater enthalpic opposition in the former compared to latter [7.5(±0.7) kJ mol^{-1} in **1** and 9.6(±0.5) kJ mol^{-1} in **3**, Table 6], thereby showing comparable ΔG_{298K}^{H-bond} [7.5-(±0.9) kJ mol^{-1} in **1** and 8.4(±0.7) kJ mol^{-1} in **3** at 298 K]. A similar analysis with methylene protons of 3′-ethyl phosphate moiety in **1** also gave comparable ΔG_{298K}^{H-bond} of 7.3 kJ mol^{-1} (Table 6), showing that the nonequivalency of the methylene protons in 3′-ethyl phosphate moiety in **1** indeed results from intramolecular H-bonding

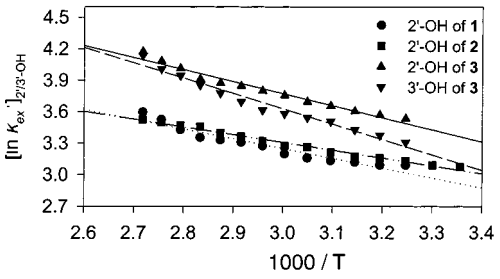

Figure 5. Activation enthalpy ($\Delta H^{\ddagger}$) and entropy ($\Delta S^{\ddagger}$) were calculated, respectively, from slope and intercept of the plot of ln k_{ex}^1, as calculated from the line shape analyses (see Table 2 and the Experimental Section for details), as a function of inverse of the temperature. The free energy of activation, $\Delta G^{\ddagger}$ at 298 K ($\cong -\Delta G_{298K}^{H-bond}$ for intra- and intermolecular H-bonding) has been calculated by using the equation viz. $\Delta G^{\ddagger} = \Delta H^{\ddagger} - T\Delta S^{\ddagger}$ on the basis of reaction rate theory.[11c,d] The plot of the [ln k_{ex}^1]$_{2'-OH}$ and [ln k_{ex}^1]$_{3'-OH}$ for adenosine 3′-ethyl phosphate (**1**), 3′-deoxyadenosine (**2**), and adenosine (**3**) as a function of the inverse of the temperature (1000/T, in K^{-1}) gives straight line with slope = −0.93 ($\sigma = \pm 0.08$), intercept = 6.04 ($\sigma = \pm 0.23$), and R = 0.96 for 2′-OH of **1** (●); slope = −0.73 ($\sigma = \pm 0.03$), intercept = 5.53 ($\sigma = \pm 0.08$), and R = 0.99 for 2′-OH of **2** (■); slope = −1.15 ($\sigma = \pm 0.06$), intercept = 7.22 ($\sigma = \pm 0.19$), and R = 0.98 for 2′-OH of **3** (▲) as well as slope = −1.46 ($\sigma = \pm 0.08$), intercept = 8.01 ($\sigma = \pm 0.24$), and R = 0.98 for 3′-OH of **3** (▼).

process. It is, however, noteworthy that the estimation of ΔG_{298K}^{H-bond} from the temperature-dependent multiplicity analysis of the methylene protons of the ethyl phosphate moiety in **1** show that the enthalpy is more dominant than entropy, which is completely opposite to what one observes from 2′-OH.

(D) Elucidation of the Nature of Hydration of 2′-/3′-OH in 1 and 3. We have explored the nature of hydration around the H-bonded 2′- and 3′-OH in adenosine 3′-ethyl phosphate (**1**) and adenosine (**3**) by a combination of ROESY and NOESY experiments[11e] in DMSO-d_6, containing ∼2 mol % HOD [δ_{HOD} = 3.239 ppm at 308 K], which allows us to make a distinction of the cross-relaxation process (chemical exchange, spin diffusion or direct magnetization transfer) between 2′-OH/ 3′-OH protons and HOD from the direct magnetization transfer process between 2′-OH/3′-OH protons and nonexchangeable protons. This has been earlier used to identify the DNA-water interaction[11e,f] in the absence of any extra catalyst. *This is, however, the first report estimating the rates of exchange of intramolecularly H-bonded 2′-OH/3′-OH protons in nucleosides and nucleotides, which can potentially be useful to understand H-bonding process in the mono- or disaccharides.* In the equilibrium of noncatalytic exchange reaction of the H-bonded 2′-OH protons in **1** and **3** at a neutral condition [2′-O−H···O3′−H(phos) + H*OD ⇌ 2′-O−H*···O3′−H(phos) + 2′-O−H···O3′−H*(phos) + 2′-O−H*···O3′−H*(phos) + HOD],[14c,d] the chemical shifts of only H-bonded hydroxyl protons are observed.

A set of NOESY experiments at 308, 318, and 348 K at τ_m = 300 ms for **1** and **3** (Figure 6) showed that the dipole−dipole magnetization transfer by cross-relaxation processes between hydroxyl protons and the nonexchangeable protons were dominant at 308 K. However, these direct magnetization transfer cross-peaks have disappeared almost completely at 348 K, while the cross-peaks due to the magnetization transfer by exchange process at the chemical shift of water (shown by an arrow in Figure 6) have increased considerably. The ROESY spectra for **1** and **3** showed a clear positive ROE contact of the hydroxyl groups with HOD over the temperature range of 308−348 K, suggesting the operation of the exchange process with water in the proximity.

The rate-limiting step of the exchange process ($k_{ex,T}^2$) is dictated by the rate of opening (k_{op}) of the 2′-O−H···O3′−H(phos) in **1** and **3**, which is expected to be very short as found for the H-bonded imino protons in the DNA duplex.[11e,f]

The relative intensities of NOE and ROE buildup curves (panels A and B in Figure 7) for the cross-peaks between the hydroxyl protons and HOD in the phase-sensitive NOESY and ROESY at 308 K at different τ_m (normalized to the diagonal intensity at τ_m = 0 ms, see Table 4) have been used to find the correct range of τ_m, where the approximations[11e] concerning the direct magnetization process (see eq 1 in the Experimental Section) is valid. Thus, this NOE/ROE buildup curve (Figure 7) showed that at τ_m = 300 ms, the cross-peaks between water and exchangeable 2′- and 3′-OH in adenosine 3′-ethyl phosphate (**1**) and adenosine (**3**) has almost zero contribution of dipole−dipole interaction, and can be used for the calculation of k_{ex}^2.

Thus, Figure 7 points to two important observations: (i) The hydration of either 2′-OH or 3′-OH at 308 K in adenosine (**3**) is relatively less compared to that of 2′-OH in adenosine 3′-ethyl phosphate (**1**). (ii) The presence of hydrophilic 3′-phosphate group in **1** causes a much higher water activity at low temperature in the vicinity of 2′-OH, which in turn causes the 2′-OH to exchange faster (Table 6), culminating in a shorter exchange lifetime[11f] (τ) for 2′-OH proton with HOD in **1** ($\tau_{2'-OH}$: 489 ms) compared to that in **3** ($\tau_{2'-OH}$: 6897 ms) at 308 K.

The temperature dependency of the k'_{ex} [where $k'_{ex} = k_{ex,T}^1 - (k_{ex,308K}^1 - k_{ex,308K}^2)$], as a function of 1/$T$ (see Figure 8 and the Experimental Section for details) showed that the activation energy[11e] (E_a, Table 6) for the hydroxyl proton exchange in **3** (E_a for 2′- and 3′-OH: 48.3 and 45.0 kJ mol^{-1}, respectively) is considerably higher compared to that of 2′-OH in **1** (E_a: 31.9 kJ mol^{-1}), thereby showing some important aspects of uniqueness of 2′-OH in RNA vis-à-vis a ribonucleoside:

(a) The more water activity around the 2′-OH of adenosine 3′-ethyl phosphate (**1**) at low temperature allows its faster exchange with the bound water because of lower E_a compared to that of **3**.

(b) The relatively lower E_a of 2′-OH exchange with the bound water in **1** gives the 2′-OH more flexibility to interact with other functions, which can assist in the RNA folding, in general. In an oligo or polymeric RNA chain, one can envision that all phosphodiesters are not uniformly exposed to the bulk water due to microenvironment variation, producing a different hydration pattern around each phosphate and around 2′-OH. This means that phosphate moieties which are less exposed to the bulk water, will impose limitation to the vicinal 2′-OH for exchange possibilities with water and thereby higher E_a. This may be responsible for a gradient of E_a of the vicinal 2′-OH exchange with the bound-water, depending on the relative hydrphobicities of the microenvironment, which may constitute an ON−OFF switch for a potential interaction with other functions in the RNA, causing it to fold or unfold. Alternatively, the nucleophilicity of a specific 2′-OH can be modulated, depending

Table 4. Normalized[a] Cross Peak Volumes ($a_{HW}^{NOE}/a_{H0}^{NOE}$ from NOESY Spectra and $a_{HW}^{ROE}/a_{H0}^{ROE}$ from ROESY Spectra) as Well as Diagonal Peak Volumes ($a_{HH}^{NOE}/a_{H0}^{NOE}$ from NOESY Spectra and $a_{HH}^{ROE}/a_{H0}^{ROE}$ from ROESY Spectra) at τ_m = 300 ms at Each Temperature for Adenosine 3′-Ethyl Phosphate (1) and Adenosine (3)

	2′-OH of **1**				2′-OH of **3**				3′-OH of **3**			
	NOESY[a]		ROESY[a]		NOESY[a]		ROESY[a]		NOESY[a]		ROESY[a]	
T (K)	$a_{HW}^{NOE}/a_{H0}^{NOE}$	$a_{HH}^{NOE}/a_{H0}^{NOE}$	$a_{HW}^{ROE}/a_{H0}^{ROE}$	$a_{HH}^{ROE}/a_{H0}^{ROE}$	$a_{HW}^{NOE}/a_{H0}^{NOE}$	$a_{HH}^{NOE}/a_{H0}^{NOE}$	$a_{HW}^{ROE}/a_{H0}^{ROE}$	$a_{HH}^{ROE}/a_{H0}^{ROE}$	$a_{HW}^{NOE}/a_{H0}^{NOE}$	$a_{HH}^{NOE}/a_{H0}^{NOE}$	$a_{HW}^{ROE}/a_{H0}^{ROE}$	$a_{HH}^{ROE}/a_{H0}^{ROE}$
308	0.9847	0.2010	0.4526	0.0637	0.0487	0.5878	0.0318	0.5240	0.0459	0.5457	0.0240	0.2808
318	1.2261	0.1781	0.4294	0.0396	0.0718	0.3994	0.0494	0.3413	0.0749	0.2901	0.0463	0.3028
328	1.3737	0.1747	0.4247	0.0336	0.163	0.3084	0.0967	0.2645	0.1698	0.2706	0.0911	0.2596
338	1.8268	0.2114	0.3857	0.0298	0.215	0.2764	0.1562	0.1995	0.2668	0.2691	0.1736	0.2089
348	2.5591	0.3178	0.5330	4.3489	0.3329	0.2466	0.2215	0.1769	0.3186	0.2654	0.2074	0.1627

[a] These normalized volumes have been used for calculating k_{ex}^2 (Table 5) using eq 1. See the Experimental Section for details.

Table 5. Halfwidth ($\Delta\nu_{1/2}$, in Hz) and Corresponding Rate of Exchange (k_{ex}^1, in s^{-1})[a] as Well as NOE/ROE Volume-Based Rate of Exchange (k_{ex}^2, in s^{-1})[b] for the Hydroxyl Protons of Adenosine 3′-Ethyl Phosphate (1), 3′-Deoxyadenosine (2), and Adenosine (3) in DMSO-d_6

	2′-OH									3′-OH		
	1			**2**			**3**			**3**		
T (K)	$\Delta\nu_{1/2}$	k_{ex}^1	k_{ex}^2	$\Delta\nu_{1/2}$	k_{ex}^1	k_{ex}^2 [c]	$\Delta\nu_{1/2}$	k_{ex}^1	k_{ex}^2	$\Delta\nu_{1/2}$	k_{ex}^1	k_{ex}^2
308	7.0	22.0	2.045	10.9	22.9		8.7	34.2	0.145	8.7	27.3	0.149
318	7.2	22.6	3.084	11.7	23.9		9.8	36.8	0.184	9.8	30.8	0.173
328	7.5	23.6	3.526	12.8	26.1		11.0	40.2	0.296	11.0	34.6	0.287
338	8.4	26.4	5.302	14.2	27.6		11.8	44.6	0.578	11.8	37.1	0.584
348	8.9	28.0	8.678	15.3	29.8		13.9	48.1	0.750	13.9	43.7	0.769

[a] k_{ex}^1 has been calculated using the equation $k_{ex}^1 = \Delta\nu_{1/2}\pi$[5b]. [b] k_{ex}^2 has been calculated using eq 1;[11e] see the Experimental Section for details. [c] No NOESY/ROESY experiments have been performed.

Table 6. Thermodynamic and Kinetic Parameters Derived from ^{1}H NMR Lineshape Analyses[a] as Well as from Temperature-Dependent ROESY and NOESY Spectra[b] of Adenosine 3′-Ethyl Phosphate (1), 3′-Deoxyadenosine (2), and Adenosine (3) in DMSO-d_6

	1			**2**	**3**	
	2′-OH	3′-OCH_2–[c]	3′-OCH_2–[d]	2′-OH	2′-OH	3′-OH
$\Delta H^{\ddagger}$ [e]	7.5 (±0.7)	−8.7 (±0.4)	−4.0 (±0.4)	6.1 (±0.2)	9.6 (±0.5)	12.1 (±0.7)
$-T\Delta S^{\ddagger}$ [e]	−15.0 (±0.6)	1.4 (±0.4)	−2.7 (±0.3)	−13.7 (±0.2)	−17.9 (±0.5)	−19.8 (±0.6)
$\Delta G^{\ddagger}$ [e]	−7.5 (±0.9)	−7.3 (±0.6)	−6.7 (±0.5)	−7.6 (±0.3)	−8.3 (±0.7)	−7.7 (±0.9)
k'_{ex} [f]	2.045	[k]	[k]	[k]	0.145	0.149
E_a [g]	31.9 (±1.2)	[k]	[k]	[k]	48.3 (±3.3)	45.0 (±2.4)
τ [l]	489	[k]	[k]	[k]	6897	6711

[a,b] See Tables 4 and 5 and the Experimental Section for details. [c] From the line shape analyses of 3′-OCH_2 of 3′-ethyl phosphate moiety in **1**. [d] Similar line shape analyses have been performed in D_2O. [e] In kJ mol^{-1} at 298 K for **1**−**3** and errors shown in parentheses (see the Experimental Section for details). [f] k'_{ex} has been calculated using the equation $k'_{ex} = [k_{ex,T}^1 - (k_{ex,308K}^1 - k_{ex,308K}^2)]$ at 308 K. [g] The activation energy (E_a) for the exchange of hydroxyl protons were obtained (see Figure 8) using the Arrhenius equation: $\ln(k'_{ex}) = \ln(A) - E_a/RT$[11f] where *A* is the frequency factor. [k] No ROE/NOE experiments have been performed. [l] The lifetime of proton exchange ($\tau = 1/k'_{ex}$, in ms)[11e] at 308 K.

upon its order of hydration and type of metal ion coordination, such that a potential in-line attack to the vicinal phosphate leading to a transesterification reaction can take place. It may be noted that it is the reactivity of a specific 2′-OH out of many others in a folded poly-RNA chain that dictate the biologically ubiquitous transesterification reaction as found in the ligation of exons and excission of introns (splicing of pre-mRNA) or in the catalytic RNA cleavage reaction.

Conclusions

(1) The temperature-dependent $^3J_{H,OH}$ analysis gives an insight into the orientation of the hydroxyl protons and the role of 2′-OH as the proton donor in the intramolecular H-bonding process in nucleosides and nucleotides for the first time. Thus, we have unequivocally provided convincing evidence in adenosine 3′-ethyl phosphate (**1**) and adenosine (**3**) that the 2′-OH proton is indeed oriented toward the neighboring O3′ to form the weak intramolecular H-bond [2′-OH···O3′]. The strength of this H-bonding has been also quantified by the line-shape analysis of the hydroxyl protons (and of the methylene protons) in **1** and **3**, which have shown the entropic predominance over the enthalpic contribution to the free energy for the exchange ($\Delta G^{\ddagger}$) of the 2′- and 3′-OH in **1**−**3** in DMSO-d_6.

(2) Relatively large water activity around the 2′-OH of adenosine 3′-ethyl phosphate (**1**) at low-temperature allows a faster exchange with the bound-water compared to that of adenosine (**3**). The two limiting activation energies for the exchange with the bound-water, one for the 2′-OH in **1** and the other for that of **3**, show the role of electronegativity and the hydrophilic character of the 3′-substituent (i.e., 3′-OH vis-à-vis 3′-phosphate). This may suggest that there are perhaps internucleotidyl phosphates in a large folded oligo or polymeric RNA, where some of the phosphates are more shielded from the water than found in the monomeric **3**. In such a system, those vicinal 2′-OH will have a higher E_a for the exchange with the bound-water than the more water

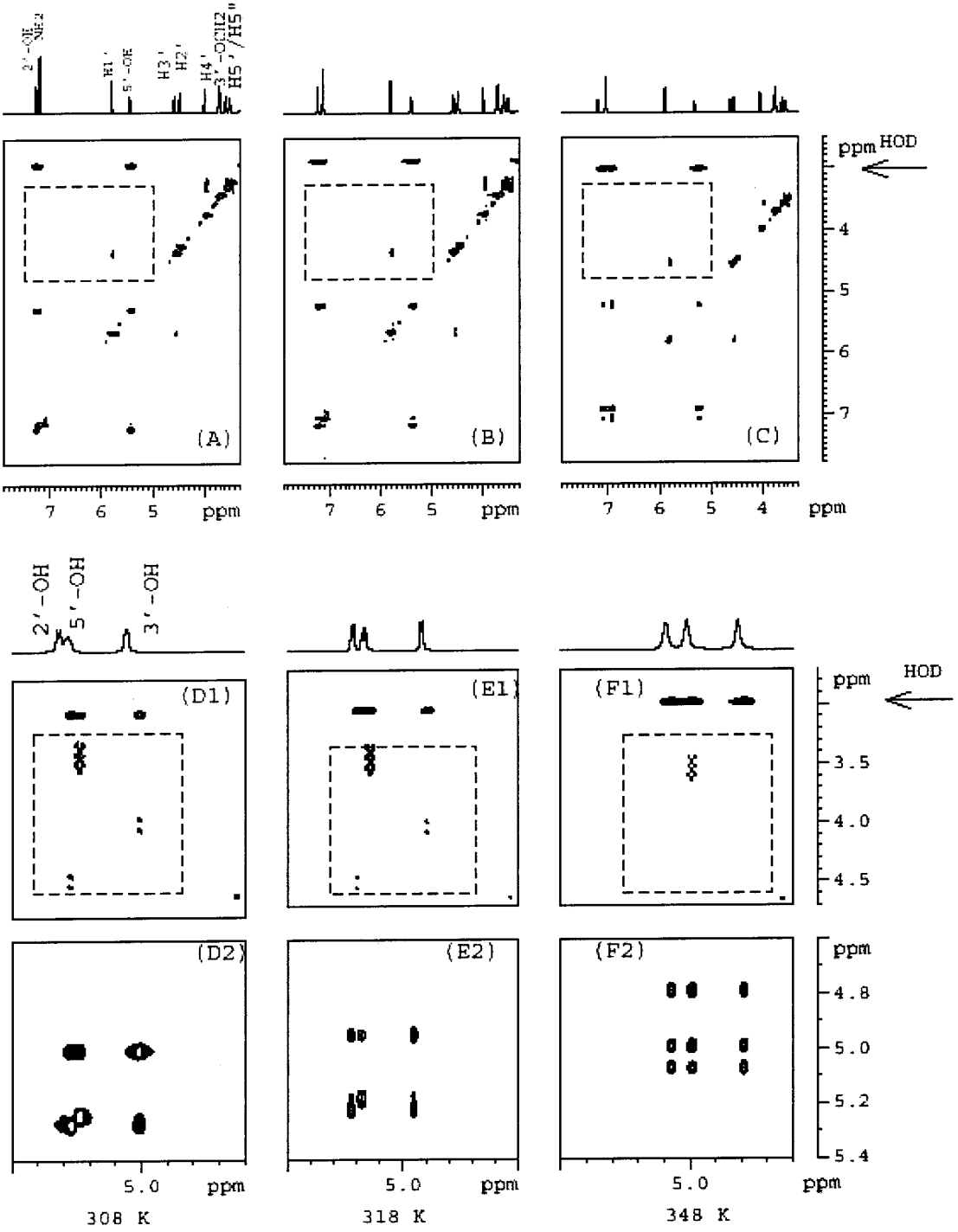

Figure 6. Panels (A−F) show the contour plots of the representative NOESY spectrum (τ_m = 300 ms) over the temperature range of 308−348 K as well as their 1D profile. The chemical shift of HOD is shown on the right with an arrow. All samples were prepared in DMSO-d_6 with a concentration of 50 mM. Panels A−C (f_1: δ7.8−2.8 ppm and f_2: δ7.9−3.3 ppm) show spectral region for adenosine 3′-ethyl phosphate (**1**) indicating that no cross-peaks for 2′-, 3′-, and 5′-OH with nonexchangeable protons have been found in the box region (the only peak found between H1′ and H2′), and cross-peaks with HOD are shown outside the box. Panels D1−F1 show the cross-peaks for 2′-, 3′-, and 5′-OH with nonexchangeable protons (f_1: δ4.8−2.9 ppm and f_2: δ5.5−4.6 ppm) in the box region (cross-peaks with HOD are shown outside the box) for adenosine (**3**). Panels D2−F2 show the diagonal peaks for 2′-, 3′-, and 5′-OH for adenosine (**3**) (f_1: δ5.4−4.6 ppm and f_2: δ5.5−4.6 ppm).

exposed phosphates, which may provide possibilities for the 2′-OH in the latter to mediate other inter or intramolecular interactions compared to the former. This suggests that the 2′-OH in native RNA can mediate other inter- or intramolecular interactions only in competition with the bound-water, depending upon the specific chemical nature and spatial orientation of other functions with potential for hydrogen bonding in the neighborhood. It is also likely that the nucleophilicity of a specific 2′-OH group is modulated by the order of its hydration due variable microenvironment, and subsequently by Mg^{2+} coordination, which may make certain 2′-OH group more prone for transesterification reaction at the vicinal phosphate function at specific sites of a folded RNA chain leading to stereoselective splicing or RNA cleavage by RNA catalysis.

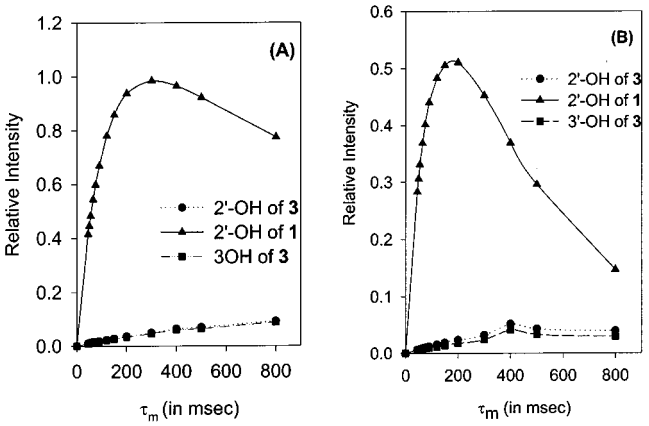

Figure 7. Panels A and B show the NOE buildup and ROE buildup curves (308 K), respectively, for the cross-peaks of 2′-OH of adenosine 3′-ethyl phosphate (**1**) as well as for 2′- and 3′-OH of adenosine (**3**) with the residual water present in DMSO-d_6 at τ_m = 45, 55, 65, 75, 150, 200, 300, 500, and 800 ms (see the Experimental Section for details), showing the relative water activity around 2′-OH in **1** and **3**.

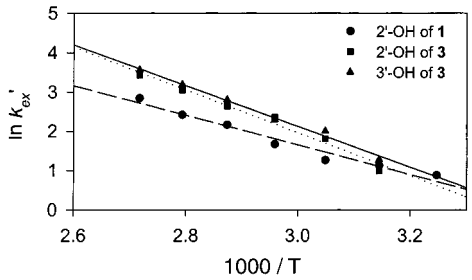

Figure 8. Arrhenius plot of logarithm of the observable rate of exchange (k'_{ex}, in s^{-1}) of hydroxyl protons of adenosine 3′-ethyl phosphate (**1**) and adenosine (**3**) (see the Experimental Section for details) as a function of inverse of temperature (1000/T, in K^{-1}) giving straight line with slope = −3.84 (σ = ± 0.29) and R = 0.99 for 2′-OH of **1** (●); slope = −5.81 (σ = ±0.39) and R = 0.97 for 2′-OH of **3** (■); slope = −5.41 (σ = ±0.14) and R = 0.98 for 3′-OH of **3** (▲). The slope of the graph gives the activation energy (E_a, in kJ mol^{-1}, see Table 6 for details).

(3) Unlike in peptide or in hexapyranose system, the subtle structural effects as well as the low energy barrier of the pentose sugar pseudorotamer interconversions due to the inherent flexibility of the saturated five-membered ring is most probably the reason for relative insensitivity of the $\Delta\delta/\Delta T$ parameter for the hydroxyl protons directly attached to the furanose system in **1**−**3** as a differentiating factor between intramolecular H-bonded state and solvated state.

(4) The concentration dependent studies have shown the self-aggregation at high concentration (>50 mM) in **1** due to the presence of negatively charged phosphate moiety. It also shows the relative ease of the solvation for the pseudoaxial OH groups (e.g., 2′-OH in **2**) compared to the pseudoequatorial one (e.g., 2′-OH in **3**).

Experimental Section

DMSO-d_6 was freshly distilled under N_2 and kept over the molecular sieves for 3 days. All the compounds, adenosine 3′-ethyl phosphate (**1**), 3′-deoxyadenosine (**2**), and adenosine (**3**) (Figure 1), were dried in desiccators under vacuum overnight.

(A) NMR Spectroscopy. All NMR experiments were performed in Bruker DRX-500 spectrometer operating at 500.1326 MHz for proton observation. The NMR samples for compounds **1**−**3** (Figure 1) were prepared in dry DMSO-d_6 solution (concentration of 50 mM) with δ_{CH_3CN} = 2.00 ppm as internal reference, and ^{1}H NMR were taken at 5 K steps over the range of 288−368 K. The assignments for the OH signals for all the compounds have been performed on the basis of selective homonuclear ^{1}H decoupling experiments. The accurate $^3J_{H,H}$ (±0.1 Hz) and $^3J_{H,OH}$ (±0.2 Hz) values were obtained through simulation using the DAISY program package (supplied by Bruker spectrospin, Germany). The NOESY and ROESY spectra for adenosine 3′-ethyl phosphate (**1**) and adenosine (**3**) were recorded in 600 MHz (Bruker DRX 600) spectrometer, in dry DMSO-d_6 solution (concentration of 50 mM) containing ∼2 mol % HOD [δ_{HOD} = 3.239 ppm] at 308 K with mixing time τ_m of 20, 45, 55, 65, 75, 90, 150, 200, 300, 500, and 800 ms. For each FID of NOESY and ROESY spectra, 16 scans were recorded with delay of 2s. The data were zero-filled to 2 × 1 K before applying a $\pi/2$ shifted sine-square bell window function in the t_1 and Lorentzian function in t_2 directions, then Fourier transformed, phase adjusted, and baseline corrected in both dimensions using polynomial.

The relative intensity of NOE and ROE buildup curves (Figure 7) for the cross-peaks between the hydroxyl protons and HOD in the phase-sensitive NOESY and ROESY at 308 K at different τ_m (normalized to the diagonal intensity at τ_m = 0 ms) has been used to find the correct range of τ_m, where the approximations[11e] concerning the direct magnetization process is valid in using the equation[11e]

$$4\left(\frac{a_{HW}^{NOE}}{a_{H0}^{NOE}}\right)-\left(\frac{a_{HW}^{ROE}}{a_{H0}^{ROE}}\right)=k_{ex}^2\,\tau_m\left[3-\left(\frac{4\,(R_{HH}^{NOE}+R_{WW}^{NOE})\tau m}{2}-\frac{4\,(R_{HH}^{ROE}+R_{WW}^{ROE})\tau m}{2}\right)\right]\ldots\ (1)$$

where $(R_{HH}^{NOE}+R_{WW}^{NOE})=\ln(a_{HW}^{NOE}/a_{H0}^{NOE})/\tau_m$ and $(R_{HH}^{ROE}+R_{WW}^{ROE})=\ln(a_{HW}^{ROE}/a_{H0}^{ROE})/\tau_m$; $(a_{HW}^{NOE}/a_{H0}^{NOE})$ and $(a_{HW}^{ROE}/a_{H0}^{ROE})$ are the cross-peak and diagonal peak intensities (see Table 4), respectively, normalized to zero mixing time intensity of the diagonal peak in the NOESY spectra (with symbol ROE in the ROESY spectra) between protons H (hydroxy) and W (water).

A combination of ROESY and NOESY experiments were used[11e,f] to calculate the rate of exchange (k_{ex}^2, with τ_m = 300 ms, see Table 5) at 308 K independently for each hydroxy proton of adenosine 3′-ethyl phosphate (**1**) and adenosine (**3**) using eq 1. These exchange rates were then subtracted from $\pi\Delta\nu_{1/2}$ (which have both magnetization and k_{ex}^2) at 308 K (the lowest temperature taken in this calculation in order to avoid the exchange contribution) to calculate the pure dipole−dipole relaxation term ($k_{ex,308K}^1 - k_{ex,308K}^2$). This dipole−dipole relaxation term was subtracted from $\pi\Delta\nu_{1/2}$ [i.e., $k'_{ex} = k_{ex,T}^1 - (k_{ex,308K}^1 - k_{ex,308K}^2)$] of all other hydroxy protons at higher temperatures (308−348 K) to calculate the pure rate of exchange (k'_{ex}) and lifetime of exchange ($\tau = 1/k'_{ex}$, in ms).[11e] The activation energy parameters for the exchange process were obtained from the plot of the pure exchange rate (k'_{ex}) as a function of temperature using Arrhenius equation: $\ln(k'_{ex}) = \ln(A) - E_a/RT$, where E_a is the activation energy and A is the frequency factor (Table 6). The error for these parameters is standard deviation (σ) of the linear regression analysis, which is shown in parentheses.

Similar NOESY and ROESY experiments have been performed for adenosine 3′-ethyl phosphate (**1**) and adenosine (**3**) over the temperature range of 318−348 K at 10 K interval with mixing time (τ_m) of 300 ms for calculating the activation energy[11f] (E_a) of exchange of hydroxy protons with residual water in the DMSO-d_6 solution using Arrhenius plot.[11e]

(B) Pseudorotational Analyses. The conformational analyses of the furanose moiety of adenosine 3′-ethyl phosphate (**1**), 3′-deoxyadenosine (**2**), and adenosine (**3**) in DMSO-d_6 have been done by the computer program PSEUROT (v. 5.4)[6a−d,7] using experimental temperature-dependent $^3J_{HH}$. It is based on the generalized Karplus equations[6a−d,7] and Pseudorotational concept[6a−d,7] (using the pseudorotation equations for the

five membered ring viz. $\nu_j = \Psi_m \cos(P + 4\pi(j-2)/5)$ [$0 \le j \le 4$] and tan $P = (\nu_4 + \nu_1 - \nu_3 - \nu_0)/3.077\nu_2$, where ν_j is the endocyclic torsion[6a−d,7]). It calculates the best fit of the five conformational parameters [P, Ψ_m for both N- and S-type pseudorotomers and the mole fractions of N (x_N) or S (x_S) conformers] to the three (or five) experimental temperature dependent $^3J_{H,H}$ (viz. $^3J_{H1'H2'}$, $^3J_{H2'H3'}$, $^3J_{H3'H4'}$ for **1** and **3**; $^3J_{H1'H2'}$, $^3J_{H2'H3'}$, $^3J_{H2'H3''}$, $^3J_{H3'H4'}$, $^3J_{H3''H4'}$ for **2**). The average slopes and intercepts derived from all van't Hoff plots were finally used to calculate the enthalpy ($\Delta H°$) and the entropy ($\Delta S°$) contributions to the free energy ($\Delta G,^{298}$ at 298 K) characterizing the N ⇆ S pseudorotational equilibrium [by plotting $\ln(x_S/x_N)$ as a function of $1000/T$].

The PSEUROT analyses for **1**−**3** in DMSO-d_6 are as follows: the sugar conformations for adenosine 3′-ethyl phosphate (**1**) and adenosine (**3**) are found to be predominantly S-type [$\Delta G^{298} = -3.9(\pm 0.2)$ kJ mol^{-1} and %S-type pseudorotamer population: 85% (288 K) and 73% (368 K) for **1**; $\Delta G^{298} = -2.1$ (± 0.2) kJ mol^{-1} and %S-type pseudorotamer population: 71% (288 K) and 60% (368 K) for **3**] with 140 °≤ $P_S \le$ 172° and 32 °≤ $\Psi_m \le$ 37° for **1** and 139° ≤ $P_S \le$ 170° and 34 °≤ $\Psi_m \le$ 39° for **3**. However, 3′-deoxyadenosine (**2**) is found to be predominantly N-type [$\Delta G^{298} = 2.3$ (± 0.2) kJ mol^{-1} and %N-type pseudorotamer population: 71% (288 K) and 65% N (368 K)] with −10 °≤ $P_N \le$ 22° and 30 °≤ $\Psi_m \le$ 40°.

(C) Thermodynamics of H-Bond Using Line-Shape Analyses from ^{1}H NMR Data. van't Hoff analyses (Figure 5) were based on the line shape analyses of the exchangeable hydroxyl protons from the ^{1}H NMR data. The line widths were determined (Table 5) by the direct reading of the full width at the half-height (halfwidth) of the 2′- and 3′-OH resonances. The rate constant for the exchange [k^1_{ex}] is related to the observed halfwidth ($\Delta\nu_{1/2}$) by the following equations:[11b]

$$k^1_{ex} = \pi^* \Delta\nu_{1/2} \qquad \text{(a)}$$

On the basis of the reaction rate theory, the thermodynamic parameters have been calculated[11c,d] from the plot of ln k^1_{ex} (assuming $k^1_{ex} = K_{eq}$) for the 2′-OH and/or 3′-OH in **1**−**3** as well as ln k^1_{ex} for the 3′-methylene protons in **1** as a function of inverse of the temperature using the van't Hoff equation assuming reaction rate theory:

$$\ln k^1_{ex} = (-\Delta H^{\ddagger}/R)(1/T) + \Delta S^{\ddagger}/R \qquad \text{(b)}$$

$$\Delta G^{\ddagger} = \Delta H^{\ddagger} - T\Delta S^{\ddagger} \qquad \text{(c)}$$

(D) Optimization of $\Phi_{H-C-O-H}$ and Molecular Modeling. The temperature-dependent $^3J_{H2',OH}$ and $^3J_{H3',OH}$ coupling constants (Table 1) for adenosine 3′-ethyl phosphate (**1**), 3′-deoxyadenosine (**2**), and adenosine (**3**) are used to calculate the torsion viz. $\Phi_{H2'-C2'-O-H}$ and $\Phi_{H3'-C3'-O-H}$ (Table 1) using the Karplus equation $^3J_{H,OH} = 10.4\cos^2\Phi - 1.5\cos\Phi + 0.2$[3]. The sugar pucker ($P$ and Ψ_m) for **1**−**3** has been calculated by pseudorotational analyse,s[6a−d,7] which in turn provides the endocyclic torsion values (ν_0−ν_1) using the pseudorotation equations.[6a−d,7] The major backbone torsions such as γ [O5′−C5′−C4′−C3′], β[P3′−O−CH_2−CH_3] for **1** have also been calculated from the respective $^3J_{H,H}$ whereas value for ε[C4′-C3′- O3′- P3′] has been calculated ($\varepsilon^- = 270°$) by pilot studies of potential energy surface scan of major ε^- (as indicated by $^3J_{H,H}$ and $^3J_{H,P}$) over the range of 240−340° at 20° steps for **1**.

The molecular model building has been done by geometry optimization with constraining NMR derived $\Phi_{H2'-C2'-O2'-H}$, $\Phi_{H3'-C3'-O3'-H}$, and sugar pucker[6a−d,7a] (see the pseudorotational analyses for details) and backbone torsions for **1**−**3** by gas-phase semiempirical AM1 and PM3 calculations and using those geometries in the ab initio gas-phase HF/Midi! and solution phase ($\varepsilon = 46.5$ at 298 K, employing PCM solvation model) HF/6-31+G*//HF/Midi! calculations as implemented in Gaussian 98[12] (Table 2) performed on DEC Alpha XP1000 work station. It provides the unique solution for energy-minimized $\Phi_{H2'-C2'-O2'-H}$ and $\Phi_{H3'-C3'-O3'-H}$ among the four probable Karplus[3] derived solutions corresponding to $^3J_{H2',OH}$ and $^3J_{H3',OH}$ for the major pseudorotamers in **1**−**3**.

For all semiempirical as well as ab initio (both gas and solution phase) calculations, the sugar geometries of **1**−**3** have been kept fixed in their major sugar pucker, i.e., S-type, N-type, and S-type, respectively [by constraining ν_0 and ν_3 (or ν_1 and ν_4)[6a−d,7] in the range of P and Ψ_m as derived from PSEUROT analyses for **1**−**3**]. The backbone torsions across ε, ζ[C3′−O3′−P3′−OEt], α[O3′−P3′−O−CH_2], and β[P3′−O−CH_2−CH_3] have been kept fixed[6d] at ε^-, α$^-$, and β^t, respectively, in all calculations for **1**. Each solution of Karplus equation (among four possible solutions of each $\Phi_{H,OH}$, see Table 1) for $\Phi_{H2',OH}$ of **1** and **2** (corresponding to $^3J_{H2',OH}$ at 298 K) has been constrained in respective geometry optimization to find the orientation of $\Phi_{H2',OH}$ at global minima for **1** and **2** (Table 2 as well as Figure 3A,B). Similarly, there are 16 different combinations possible from the Karplus derived solutions of $\Phi_{H2',OH}$ and $\Phi_{H3',OH}$ corresponding to $^3J_{H2',OH}$ and $^3J_{H3',OH}$ at 298 K of **3** (Table 1). Nevertheless, the existence of $^4J_{H2',OH3'}$ allows the possibility of only positive values of $\Phi_{H3',OH}$ (i.e., with W conformation of H2′−C2′−C3′−O3′−H) thereby values of $\Phi_{H3',OH}$ in negative cisoid and negative transoid domains (Figure 2) were neglected. So these plausible combinations of $\Phi_{H2',OH}$ and $\Phi_{H3',OH}$ have been kept constrained in respective geometry optimization to find the orientation of $\Phi_{H2',OH}$ and $\Phi_{H3',OH}$ at global minimum for **3** (Figure 3C).

(E) Conformational Grid Search for the Intramolecular H-Bonding Distances ($d_{2'OH...O3'}$). Conformational grid search for calculating intramolecular H-bonding distance ($d_{2'OH...O3'}$) has been performed by energy minimization on Silicon Graphics Indigo R4000 workstation with each AM1-optimized geometry as the starting structure (vide infra) using SYBYL (v. 6.2), based on the Tripos Force Field with Conjugate gradient method and the maximum iteration value was specified as 100 with the threshold energy of termination for the optimization as 0.05 kcal mol^{-1}.

For both **1** and **3**, the S-type conformers having energy-minimized $\Phi_{H2'-C2'-O2'-H}$ at 288 and 368 K have been taken as the starting structures. The intramolecular hydrogen-bond distance between 2′OH and O3′ [$d_{2'OH...O3'}$] has been varied over the range of 1.7−2.8 Å in 0.1 Å steps (0.05 Å steps when close to the energy minima) while constraining sugar pucker at P_S = 151.0°, Ψ_m(S) = 35.0° (average value of the calculated pseudorotational hyperspace, see the pseudorotational analyses for details), χ(anti), γ^+, ε^-, α$^-$, β^t for **1** and P_S = 159.0°, Ψ_m(S) = 36.5° (average value of the calculated pseudorotational hyperspace, see the pseudorotational analyses for details) for **3** along with $\Phi_{H2'-C2'-O2'-H}$ at 123.5° and 100.3° corresponds to the respective $^3J_{H2',OH}$ at 288 and 368 K for **1** and χ(anti), γ^+, $\Phi_{H2'-C2'-O2'-H}$ at 133.2° and 102.4° as well as $\Phi_{H3'-C3'-O3'-H}$ at 125.1° and 76.8° respectively corresponds to the respective $^3J_{H2',OH}$ and $^3J_{H3',OH}$ at 288 and 368 K for **3**.

Acknowledgment. We thank the Swedish Board for Technical Development (TFR), the Swedish Natural Science Research Council (NFR), and the Swedish Board for Technical Development (NUTEK) for generous financial support. Thanks are due to the Wallenbergstiftelsen and the University of Uppsala for funds to purchase of 500 and 600 MHz Bruker DRX NMR spectrometers.

Supporting Information Available: Figure S1: Schematic representation of all compounds **1**−**4**. Figure S2: van't Hoff plot based on line shape analyses of methylene protons of 3′-ethyl phosphate moiety in **1**. Figure S3: Concentration-dependent δ_{OH} of **1**−**3**. Figure S4: Normalization curve for cross and diagonal peaks from NOESY and ROESY spectra of **1** over the temperature range of 308−348 K. Figure S5: Normalization curve for cross and diagonal peaks from NOESY and ROESY spectra of **3** over the temperature range of 308−348 K. Table S1: Temperature-dependent δ_{OH} for **1**−**4**. Table S2: Concentration-dependent δ_{OH} for **1**−**4**. Table S3: Temperature-dependent $^3J_{H,H}$ for **1**−**4**. Table S4: Temperature-

dependent $^3J_{H,OH}$ for **1**−**4** and respective $\Phi_{H,OH}$. Table S5: Grid search for energy-minimized intramolecular H-bond distance [$d_{2'OH...O3'}$] of **1** and **3** using Molecular Mechanics (MM) by Sybyl (v. 6.4). Tables S6−S8: Temperature-dependent line shape analyses for **1**−**3**. Table S9: Pseudorotational analyses for **1**−**4**. Tables S10−S15: Torsional hyperspace calculations for $\Phi_{H2',OH}$ and $\Phi_{H3',OH}$ for **1**−**3** using semiempirical as well as ab initio (both gas and solution phase) calculations as implemented in Gaussian 98. Tables S16−S19: The diagonal peak volumes and the normalized diagonal and cross-peak volumes as calculated from NOESY and ROESY spectra using AURELIA for **1** and **3**. Table S20: The exhange rate (k^2_{ex}) of hydroxyl protons from temperature-dependent NOESY and ROESY in **1** and **3**. Experimental section (parts A−E) giving details of all NMR and computational procedure and part F providing coordinates of energy minimum for compounds **1**−**3**. This material is available free of charge via the Internet at http://pubs.acs.org.

JO010960J